Tampere University

Lari Kuuppo

THE EFFECT OF THE STRUCTURE IN CONTROLLING RESISTIVITY AND PERMITTIVITY OF 3D PRINTED ELECTROMAGNETIC ANALOGUE OBJECTS

Master of Science Thesis
Faculty of Engineering and Natural Sciences
October 2020

ABSTRACT

Lari Kuuppo: The Effect of the Structure in Controlling Resistivity and Permittivity of 3D Printed Electromagnetic Analogue Objects
Master of Science Thesis
Tampere University
Master's Degree Programme in Materials Science
October 2020

The objective of this thesis was to study how the structure affects to resistivity and permittivity of a 3D printed analogue object. This was done by creating analogue objects with different mesh structures, layer thicknesses and triangle sizes in MatLab using certain algorithms and 3D printing the objects using FDM method. Also solid objects were printed. After that resistance of the objects was measured, resistivity calculated, and the inner structure of the objects examined by optical microscope and permittivity calculated.

It was found that the nozzle temperature in 3D printing affects the adhesion between the layers and thus to resistivity: the higher the temperature the better the adhesion and lower the resistivity. It was also found that the properties of a 3D printed objects are anisotropic - resistivity is lower in lateral direction than in perpendicular direction: electric current is easier to pass through layers in lateral direction because it cannot jump from one layer to another in perpendicular direction. It also matters whether the object is mesh or solid: resistance is higher in mesh structure than in solid structure because the cross-section of the solid structure is bigger - solid structure has more material along which an electric current can flow, and thus the resistivity of solid objects is lower. The layer thickness of the object effects the properties: the larger the layer thickness, the more space there is inside the printed object. Also, it can be said that when using thicker layer thickness, tiny gaps will be harder to fill. The more there is empty space inside the object the higher the resistivity and the lower the permittivity.

When comparing the obtained resistivity values to the resistivity values of different human tissues can be seen that some of the resistivity values of the printed objects correspond well to some of the tissue resistivity values. Based on this study, it can be said that it is possible to predict the resistivity of a solid 3D printed object. Also, the effect of different 3D printing parameters on the amount of an empty space inside of an object is better known.

Keywords: 3D printing, FDM, resistivity, permittivity.

TIIVISTELMÄ

Lari Kuuppo: Rakenteen vaikutus 3D-tulostettujen sähkömagneettisten analogisten kappaleiden resistiivisyyden ja permittiivisyyden hallinnassa
Diplomityö
Tampereen yliopisto
Materiaalitekniikan diplomi-insinöörin tutkinto-ohjelma
Lokakuu 2020

Tämän diplomityön tarkoituksena oli tutkia kuinka 3D-tulostetun kappaleen erilaiset ominaisuudet ja rakenne vaikuttavat sen resistiivisyyteen ja permittiivisyyteen. Tutkimuksessa luotiin tiettyjen algoritmien avulla kappaleita MatLab:ssa. Kappaleilla oli erilainen sisäinen kolmioista koostunut verkkorakenne, jossa kerroksen paksuus ja kolmion koko vaihtelivat. Nämä kappaleet tulostettiin FDM-menetelmää käyttäen. Myös kiinteitä kappaleita tulostettiin. Tämän jälkeen niiden resistanssi mitattiin ja resistiivisyys laskettiin, sekä sisäinen rakenne tutkittiin optisella mikroskoopilla ja permittiivisyys laskettiin.

Huomattiin, että suuttimen lämpötila 3D-tulostuksessa vaikuttaa kerrosten väliseen adheesioon ja siten resistiivisyyteen: mitä korkeampi lämpötila, sitä parempi adheesio ja matalampi resistiivisyys. Huomattiin myös, että 3D-tulostetun kappaleen ominaisuudet ovat erilaiset kerrosten suunnassa kuin niitä kohtisuoraan vastassa olevassa suunnassa - resistiivisyys on matalampi kerrosten suunnassa kuin kohtisuorassa suunnassa: sähkövirran on helpompi kulkea kerroksia pitkin kuin hypätä kerrokselta toiselle kohtisuorassa suunnassa. Myös sillä on merkitystä, onko kappale verkkorakenteinen vai kiinteä: resistanssi on korkeampi verkkorakenteessa kuin kiinteässä rakenteessa, koska kiinteän rakenteen poikkipinta-ala on suurempi. Näin ollen kiinteässä rakenteessa on enemmän materiaalia, jota pitkin sähkövirta voi kulkea ja siksi kiinteän kappaleen resistiivisyys on matalampi. Kappaleen kerrospaksuus vaikuttaa sen ominaisuuksiin: mitä suurempi kerrospaksuus, sitä enemmän kappaleen sisällä on tyhjää tilaa. Voidaan myös sanoa, että kun käytetään suurempaa kerrospaksuutta, pieniä koloja on vaikeampi täyttää. Mitä enemmän kappaleen sisällä on tyhjää tilaa, sitä korkeampi on resistiivisyys ja matalampi permittiivisyys.

Kun verrataan kappaleista mitattuja resistiivisyyden arvoja tiettyjen kudosten resistiivisyyden arvoihin, voidaan nähdä, että jotkut saadut arvot ovat hyvin lähellä kudosten arvoja. Tämän tutkimuksen perusteella voidaan sanoa, että 3D-tulostetun kappaleen resistiivisyys on mahdollista ennustaa. Myös 3D-tulostuksen parametrien vaikutus kappaleiden sisällä olevan tyhjän tilan ja ilman määrään tiedetään paremmin.

Avainsanat: 3D-tulostus, FDM, resistiivisyys, permittiivisyys.

PREFACE

This thesis was done in the Faculty of Materials Science of Tampere University in collaboration with the Department of Mathematics. I am grateful to Associate Professor Sampsa Pursiainen for the opportunity to do this thesis.

I would like to express my sincere gratitude to my supervisors Assistant Professor Essi Sarlin and Associate Professor Sampsa Pursiainen. Essi gave me good feedback to improve this thesis and a lot of encouraging advice when I needed it. Sampsa tirelessly followed the progress of this thesis, gave good feedback and helped with the mathematics. Their guidance was a vital part of completing this thesis.

I would like to thank Senior Laboratory Technician Mika Kiirikki for his friendly help and valuable advice in 3D printing. Likewise, I appreciate the help of Senior Laboratory Technician Petri Virta. I also want to thank Research Engineer Merja Ritola for her help in preparing the samples and using the microscope.

In addition, I want to thank my fellow students for their peer support and making my years of study unforgettable: Katja, Liisa, Mira, Karoliina, Lucas, Antti, Santtu, Rulis, Pauli and Aku.

Finally, I want to thank my sister Liisa and her family for all the love, support and encouragement. We have gone through a lot together.

Glory to Thee, our God, glory to Thee.

This thesis is dedicated to my father Martti, who passed away during my studies.

Tampere, 18th of October 2020

Lari Kuuppo

CONTENTS

LIST OF FIGURES

LIST OF TABLES

LIST OF SYMBOLS AND ABBREVIATIONS

A	Cross-sectional area of the specimen
a	Degree of the mixing model
°C	Degrees of Celsius
ε	Dielectric constant
ε_i	Complex permittivity of the inclusion material
ε_m	Complex dielectric constant of two-component mixture
ε_R	Dielectric constant
ε_R'	Real part of the dielectric constant
ε_R''	Imaginary part of the dielectric constant or attenuation parameter
i	Imaginary constant
φ	Volume fraction of the inclusions
kΩ	Kilo ohms
l	Length of the specimen or the evaluation length
m	Meter
m^2	Square meter
ω	Angular velocity
Ω	Ohm
Ω·cm	Ohm centimetre
Ω·m	Ohm metre
ρ	Electrical resistivity
R	Electrical resistance
Ra	Surface roughness
S/m	Siemens per metre
σ	Electrical conductivity
$tan\,\delta$	Loss tangent
$Z(x)$	Height of the assessed profile at any position x

2D	Two dimensional
3D	Three dimensional
ABS	Acrylonitrile-butadiene-styrene
Avg.	Average
CAD	Computer Aided Design
COV	Coefficient of Variation
CPC	Conductive Polymer Composite
DC	Direct Current
FDM	Fused Deposition Modelling
Hz	Hertz
PLA	Polylactide
SLA	Stereolithography
SLM	Selective Laser Melting
SLS	Selective Laser Sintering
St. Dev.	Standard Deviation
STL	Stereolithography

1. INTRODUCTION

There are many situations in which human senses or even technical devices are unable to provide accurate information about objects or phenomena of interest. Problems occur when the object or process cannot be accessed or reached for observation. For example, there are problems of geophysical research, problems of astrophysics in astronomy, problems of medical diagnostics, and many others. The main aspect of the describing of experimental results for all these problems is that we must conduct results from indirect indications of the object that can be measured experimentally. For example, an image in computer tomography has to be calculated. If the results of the observations are known, the causes have to be concluded. An inverse algorithm is used for this purpose. [1]

An inverse algorithm is a mathematical model. It is essential to investigate how well the model corresponds to reality. Therefore, a real analogue object has to be made for the model and study its characteristics. The conductive nature of human tissue can be utilized in medical diagnostics. Therefore, it is crucial to understand how the model which describes the resistivity of a tissue corresponds to reality. In the Table 1 are shown conductivity and resistivity values of some human tissues.

Table 1. *Conductivity and resistivity of different human tissues [2]*

Human tissue	Conductivity [S/m]	Resistivity [Ω·cm]
Cerebrospinal fluid	1.79	56
Gray matter	0.33	303
Skin	0.33	303
Skull	0.0042	23810
White matter	0.14	714

Analogue models can be made by Fused Deposition Modelling (FDM). FDM is one of the rapid prototyping methods. Rapid prototyping is more cost-effective than the traditional prototyping methods such as wood turning or machining. Amongst the rapid prototyping methods FDM is considered as an additive manufacturing method which can be automatized and is precise and economical. FDM can be used to make solid objects with complex geometric shapes using thermoplastic as a raw material. The process proceeds

layer by layer relatively fast thus reducing cycle time and costs. The other main advantages are a large variety of thermoplastic materials available, easiness of material change, no supervision needed during the manufacturing and theoretically good absolute tolerance. [3]

As mentioned previously, polymers are used as raw materials in FDM. Polymers have many advantages compared to other materials, such as metals. A very wide variety of different kinds of polymers is available and thus there are many options to choose the most suitable from. In addition, the properties of polymers can easily be modified. For example, conductivity and permittivity of polymers can be changed by the use of certain fillers or additives: conductivity can be modified using carbon black or carbon nanotubes, permittivity can be modified using ceramics.

This study focuses on examining the effect of material properties and structure in controlling the resistivity and permittivity of 3D printed electromagnetic analogue objects. This is done by studying how different 3D printing parameters affect the empty space inside the object and resistivity of the object. Also, one focus is to create an object and study how its electromagnetic properties correspond to the electromagnetic properties of a certain human tissue (i.e. reality).

Certain algorithms in MatLab are used to create objects with different mesh structures. Also, solid objects without mesh structure are created. Two types of polymeric-based filaments with modified properties are used as raw material from which the studied objects are made using FDM. The resistance of the objects is measured, and resistivity calculated based on the measurements. The obtained resistivity values are compared to the resistivity values of different human tissues. If the resistivity of the measured object corresponds to the resistivity of the tissue, it can be said that the analogue model corresponds well to reality. From this it can be further concluded that the mathematical model corresponds well to reality.

Also, the inner structure (adhesion between the layers and possible porosity) of the object is examined using optical microscope. The results of the examination are compared to the results of the resistivity and permittivity calculations of the object to see how the inner structure affects the electromagnetic properties. If the results correspond to each other, it can be said that the analogue model corresponds well to reality. In this study the obtained results of the analogue objects were compared with the already existing data

of the resistivity of a certain human tissue. If the results of the analogue objects correlate to the existing data it can be concluded that the analogue model corresponds to reality.

2. VALIDATION OF FORWARD AND INVERSE ALGORITHMS

Nowadays, mathematical modelling is used in many fields to describe and investigate various processes or objects. Most often it is used in natural and engineering sciences, such as biology, physics, and biosciences. It can be said that a mathematical model is “a representation of the essential aspects of an existing system (or a system to be constructed) which presents knowledge of that system in usable form” [4]. Mathematical models can be diverse: dynamic systems, statistical models, differential equations or inverse and forward algorithms.

Inverse algorithm is an algorithm which describes an inverse problem - it is a mathematical model of the inverse problem. The model is valid only if it is an accurate representation of reality. If it is not, then it is invalid. There are various methods to perform the validation. In general, in validation two results are compared: the results of the model have to be compared to the results of the real world. If the comparison is true, then the model is valid. The most reliable way to validate the model is to compare the results directly to the real world. However, in practise this is impossible in most of the cases because the measurements of the real system would be too expensive to perform, or the real system is inaccessible. [5]

A better way to validate a mathematical model is to design and create an analogue model of the problem the mathematical model describes. If permittivity and conductivity are to be modelled using mathematical modelling, a mesh structure can be used for modelling permittivity and conductivity of an object. In addition, permittivity and conductivity of the material from which the model is made must be known.

After creating the analogue model, permittivity and conductivity of the analogue model have to be measured. After that, the results have to be compared to reality. However, it might be possible that neither of the models describe the real world accurately. Therefore, a large amount of discretion must be used when validating models against the results of other models.

3. ELECTROMAGNETIC PROPERTIES OF PLASTICS

In this chapter will be discussed the theory of conductivity of conductive polymer composite as well as the permittivity of polymers.

3.1 Theory of conductivity of conductive polymer composite

Electrical conductivity in a medium is a result of the movement of electrically charged particles - electrons. Metals have a crystalline form at the molecular level in which the outermost electrons of each atom are rather loosely bound. That allows the electrons to be shifted from atom to atom with relatively little force and it makes the material conductive. Usually, polymers conduct electricity poorly as such, and therefore they are regarded as insulators. The molecules of polymers are hold together by strong covalent bonds formed by shared electrons. Because electrons are held tightly, their movement from one molecule to another requires a lot of force, and therefore, polymers are insulators. [6, 7]

If it is desired for the polymer to become electrically conductive, electrically conductive substance must be added to it. Conductive filler can be carbon black, carbon fibres or carbon nanotubes or any kind of filler which creates conducting paths through the polymer matrix. The morphology and the structure of the conductive paths are the most important factors for good electrical conductivity of conductive polymer composite (CPC). [8] In the Figure 1 is shown the distribution of the conductive fillers in a polymer composite A) a non-conductive polymer at low filler content, and B) a conductive polymer with conductive paths at high filler content.

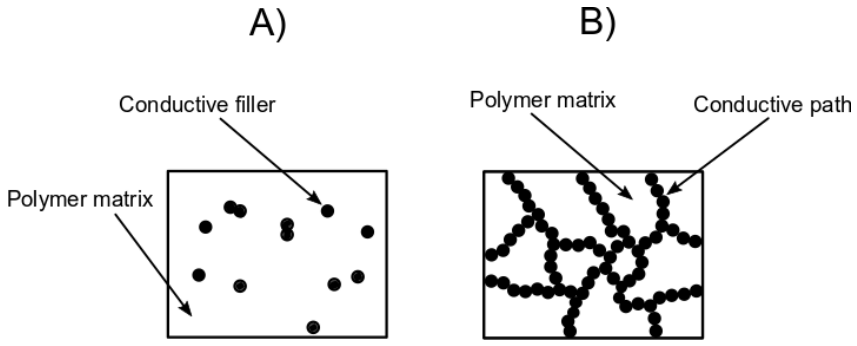

Figure 1. *Filler distribution in polymer matrix, adapted from [9]*

Predicting the electrical conductivity of conductive polymer composites has proved difficult. The electrical properties of these materials have been explained by many models. So far, the percolation theory is the best theory to describe the conductivity of CPC. The theory is divided into two prime sections: below and above the percolation threshold. There are fundamental differences in conductive behaviour below and above the threshold. In the area below the percolation threshold, the filler loading is low, and the particles are randomly dispersed and do not form conductive paths throughout the matrix. Therefore, the electrical conductivity corresponds to the electrical conductivity of the polymer matrix. As the filler content increases, unending conductive paths are built until the percolation threshold is reached. Above the percolation threshold, the amount of the conductive paths progresses at the same pace as the filler concentration develops until the electrical conductivity plateau is reached. For a polymer to be electrically conductive, the percentage of the conductive filler must be above the percolation threshold. [8, 10, 11] In the Figure 2 is shown the schematic presentation of the percolation curve.

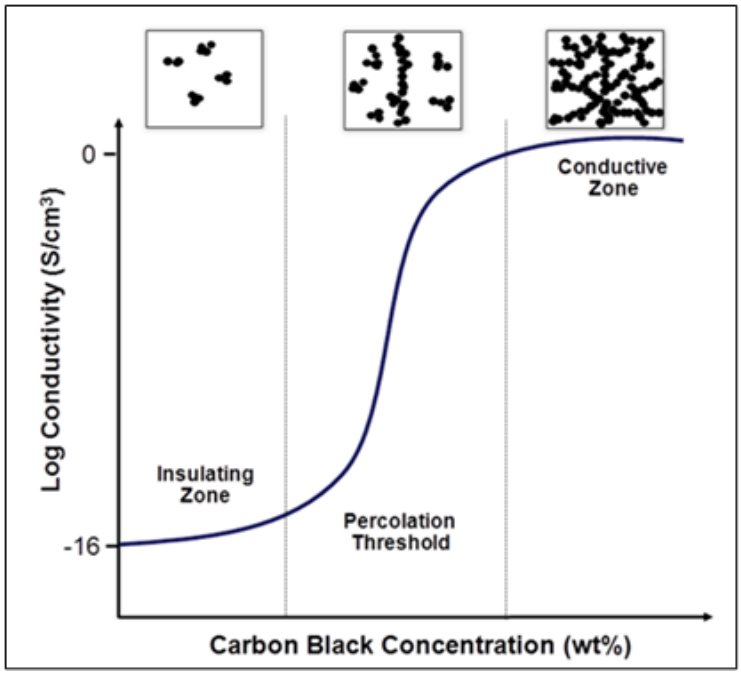

Figure 2. *The percolation curve [12]*

There are several other factors that have effect on the conductivity of CPCs. The electrical conductivity of the filler is obviously one significant factor in determining the conductivity of the CPC. Also, the particle size of the filler affects the conductivity: the smaller the particle size the lower the percolation threshold. The aspect ratio of the filler has an effect on the conductivity. Lower percolation threshold occurs if the aspect ratio is greater

than one or if the range of the aspect ratios is wide. Conductivity and percolation threshold are greatly affected by the surface properties of the polymer and the filler because the interaction between the filler and the matrix is influenced by the surface free energies: it can be said that the smaller the difference between the surface energy of the filler and the matrix the better electrical conductivity is obtained. In many cases fillers are aggregated in particles. These aggregates have to be separated to obtain good dispersion because the filler has to be dispersed as homogenously as possible to achieve good conductivity. [13, 14, 15]

Nowadays, carbon black and carbon fibres are the most used conductive fillers in conductive polymer composites. Compared to other conducting fillers, carbon black has a greater tendence to comprise conductive paths than other conductive substances, such as metal powder or flakes. Also, carbon black has other advantages, such as light weight, low cost, and permanent conductivity, making it very popular among conductive fillers. [16, 17]

When talking about a 3D printed object, it has to be kept in mind that the structure of a 3D printed object is not homogeneous when viewed horizontally and vertically. It is because the 3D printing process proceeds in layers from bottom to top. This causes anisotropic conductivity within the object, which means that conductivity is greater in one direction than in the other. Usually, the conductivity is bigger in x/y-direction (side-side) than in z-direction (top-bottom). [14]

3.2 Permittivity of polymers

Permittivity describes how an electric field affects a medium. When material is affected by an electric field, it stores the electrical potential energy. Permittivity is the ability of the material to store the energy – it is the measure of how much the electric field interacts with the medium and how much the medium is polarized. High permittivity indicates that the medium is capable of storing large amount of energy. Permittivity is also called dielectric constant and is denoted typically by ε. Permittivity is dimensionless. [18]

If the electric field is periodically changing, complex permittivity is used to describe the permittivity during a periodic variation of the electric field. It can be written as follows

$$\varepsilon_R = \varepsilon_R' + i \cdot \varepsilon_R'' = \varepsilon' + i \cdot \frac{\sigma}{\omega} \quad (1)$$

where ε_R is permittivity, ε_R' is the real part of permittivity, i is the imaginary number, ε_R'' is the imaginary part of permittivity, σ is electrical conductivity, ω is angular velocity of the applied electric field $(= 2 \cdot \pi \cdot frequency)$.

The real part refers to the ability of the material to store the electric energy – it is an indication of the degree of polarization. The imaginary number extends the real number system to the complex number system. The imaginary part represents the dielectric loss in the material and is also called the attenuation parameter. Here, $\varepsilon_R'' = \sigma/\omega$ is the loss term, which can be controlled by a mesh structure in mathematical modelling. Conductivity can be calculated using the imaginary part of permittivity and angular velocity as follows

$$\sigma = \varepsilon_R'' \cdot \omega \tag{2}$$

Loss tangent is the tangent of the angle between the resistive component and reactive component of an electromagnetic field. The loss tangent can be considered as the ratio of the imaginary permittivity to the real permittivity. [19] A large loss tangent means that there is a lot of dielectric absorption. The loss tangent can be written as follows

$$\tan\delta = \frac{\varepsilon_R''}{\varepsilon_R'} \tag{3}$$

In general, permittivity is complex and depends on the dielectricity and conductivity of the material. In plastics, the permittivity can best be explained by how easily the plastic molecules can be polarized. Low permittivity is required when plastics are used as insulators and as insulating materials. Temperature, moisture, electrical frequency and part thickness affect permittivity. Also, the structure of a polymer affects the permittivity. Polar plastics absorb moisture from the air. The moisture increases permittivity and decreases resistivity. [20]

Permittivity of a polymer is low, and it is difficult to improve. Typically, the permittivity of unfilled ABS (Acrylonitrile-butadiene-styrene), which is very commonly used material in 3D printing, measured at 100 Hz is 2.9 - 3.4. As a comparison, relative permittivity of the vacuum is 1. Inorganic fillers with good dielectric properties must be added to it to increase the permittivity. Usually, ferroelectric ceramic fillers are used for that purpose. The loading fraction and distribution of ceramic fillers determine the dielectric properties of the polymer composite. Usually, the main factor affecting the dielectric performance is the filler concentration. Therefore, the percolation theory can be applied to permittivity of plastics as well. [21]

3.3 Mixing model

If the permittivity of a material cannot be measured or determined experimentally, a mathematical model can be used to estimate it. When the studied material is a mixture and consists of more than one component, a mixing model can be used to estimate the permittivity of the mixture. [22, 23] One mixing model described by Sihvola et. al. can be written as follows

$$\varepsilon_m = (1 - \varphi + \varphi\varepsilon_i^a)^{1/a} \quad (4)$$

where ε_m is the complex dielectric constant of two-component mixture, φ is the volume fraction of the inclusions, ε_i is the complex permittivity of the inclusion material, a is the degree of the model. [24]

3.4 Filaments with customized electromagnetic properties

Nowadays, polymers with tailored electromagnetic properties are well available. Also, filaments for 3D printing with customized electromagnetic properties are manufactured. In the Table 2 are shown some of the manufacturers as well as their products.

Table 2. *Filaments with tailored electromagnetic properties*

Manufacturer	Filament	Tailored property
Graphene Laboratories Inc. [25]	BlackMagic3D	Conductivity
Multi3D [26]	Electrifi	Conductivity
Premix [27]	PrePerm®	Permittivity
Protoplant [28]	Proto-Pasta	Conductivity

4. RESISTANCE MEASUREMENT OF CPC

The electrical properties of polymers are defined by volume resistivity or specific volume resistance. According to Ohm's law, volume resistivity is represented as "the ratio of DC voltage applied between two electrodes to the resulting current through the specimen, the electrodes being located on opposite surfaces of the specimen". [29]

Several standards define how resistance or resistivity of conductive plastics is measured, i. a. standards ISO 2878:2011, ISO 3915:1981 and ISO 1853:2011. Specimens measured according to these standards have to be made in a specific way. If the specimens are not manufactured according to the standards, the standards cannot be applied in the resistance measurements, as in this study.

A basic way to measure the electrical resistance of an object is to use a standard commercial multimeter. The idea is that the multimeter places a voltage at the two electrodes and this will cause a current to flow in the object which resistance is being measured. By this way, it is possible to determine the resistance between the two electrodes and thus the resistance of the measured object.

Electrical contact resistance must be considered when measuring the resistance of an object. Contact resistance refers to the resistance at an interface between two conductors: in resistance measurement at an interface between the electrode and the measured object. No matter how thin the interface between the two elements is, it is always considered as resistor when it is seen as a circuit element and therefore it affects the measured resistance values.

When looking on the microscale, all solid surfaces are rough. Therefore, contact between two objects is restricted to a few actual contact areas. This is followed by the fact, that the actual contact area is a small fraction of the nominal contact area. If an electrical current flows between two contacting bodies, it has to pass through these small areas, causing an electrical contact resistance. Thus, contact resistance changes as a function of contact area: contact resistance increases when contact area decreases. [30] In Figure 3 is shown a schematic presentation of an electrical interface between the surfaces of two bulk objects.

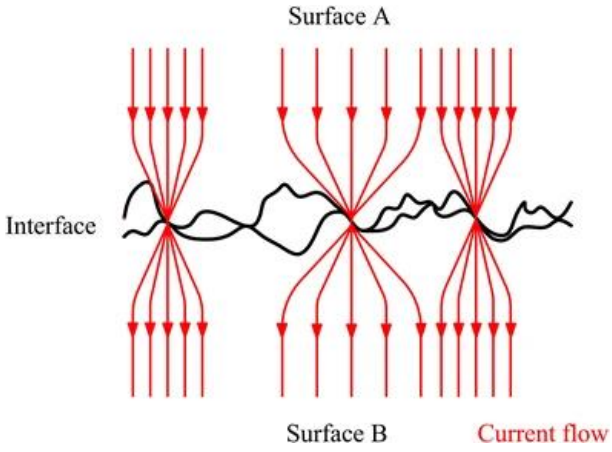

Figure 3. *An electrical interface between the surfaces of two bulk objects. [31]*

Also, contact resistance depends on the load applied to the measured object when it is pressed against the electrodes. The heavier the load, the larger the contact area and the lower the contact resistance. In addition, an electrolyte can be used to decrease the contact resistance at the interface of the electrodes and the measured object. An electrolyte, for example an electrode gel, is an ionic conductor that conducts the electric current. It acts as a conductor between the electrode and the object and thus decreases the contact resistance. Also, electrolyte gel reduces the effect of the surface roughness by penetrating the “valleys” between the layers and thus decreasing the contact resistance.

The electrical resistivity of a material is defined as the resistance of the material multiplied by its cross-sectional area per unit length at a specified temperature. Resistivity is useful when different materials are compared based on their ability to resist or conduct an electric current. Conductivity and resistivity are inversely related to each other: high resistivity means bad conductivity.

In an ideal case where cross section and composition of the sample are uniform throughout the sample the resistivity is calculated by the following equation:

$$\rho = R\frac{A}{l} \tag{5}$$

where ρ is resistivity [$\Omega\cdot\mathrm{m}$], R is the electrical resistance of a uniform specimen of the material [Ω], A is the cross-sectional area of the specimen [m^2], l is the length of the specimen [m]. [32]

When the case is less ideal, for example the geometry is more complicated, more general expression has to be used. However, general expression was not used in this study

even though the geometry is complicated. In this study, the resistance of a cube shaped object was measured. Therefore, the expression can be simplified to $\rho = R\frac{A}{l} \rightarrow \rho = R\frac{l \cdot l}{l} \rightarrow \rho = R \cdot l$. Using this simplified equation, the differences caused by the internal structure of the object become apparent.

5. 3D PRINTING OF PLASTICS

Over the last 10-15 years, rapid prototyping has grown in popularity. Computer aided design (CAD) has evolved, thus making designing and prototyping easier and more accessible to a larger number of people. Also, rapid prototyping methods have been developed. Many rapid prototyping applications are additive manufacturing, which makes it faster and less expensive than subtractive manufacturing. Nowadays, rapid prototyping methods can be used for plastics, metallics and ceramics. There are many different methods for plastics, for example stereolithography (SLA) and selective laser sintering (SLS). This study focuses on fused deposition modelling (FDM).

Additive manufacturing is an opposite of subtractive manufacturing. In additive manufacturing material is added instead of subtracted. Additive manufacturing is known as 3D printing commonly. The 3D printing process begins by creating a CAD model of the printed object. After that, the model is converted into STL format. In Figure 4 is shown a STL model of an object in a wireframe view. The wireframe view is a view where all the edges of the object are visible. [33, 34]

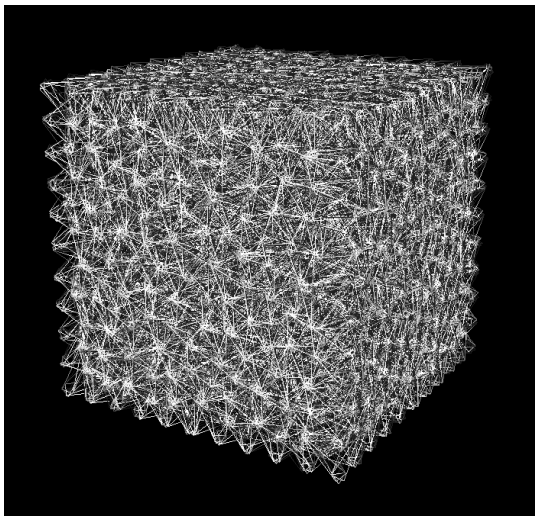

Figure 4. *A STL model of an object in a wireframe view*

Usually, the next step is to manipulate the model so that it can be executed by the printer. After that, the printer has to be properly set up for the building process. Once the set-up is done, the printing of the object is an automated process and can be done without

supervision. After completing the printing, the object must be removed from the printer. If desired, post-processing can be done on the object. [35, 36]

Nowadays, the most widely used technology in 3D printing of plastics is fused deposition modelling (FDM). FDM is a process based on extrusion. The basic principle of the process is to load, melt and extrude molten polymer through a nozzle plotting it according to a certain path in a controlled manner. The filament is heated so hot that it melts, i.e. above its melting point (semi-crystalline polymer) or glass transition temperature (amorphous polymer). Then it is extruded on x-, y- and z-stage to build a 3D object. Once the melt filament is plotted, the material adheres to previous layer and hardens immediately to build a solid structure. The characteristic features of FDM technology are that a heating chamber is used for melting the polymer which is fed into the chamber as filament. A tractor wheel pushes the filament into the chamber, and the pushing produces the extrusion pressure. [33, 34, 35] In Figure 5 is shown a schematic presentation of the FDM process.

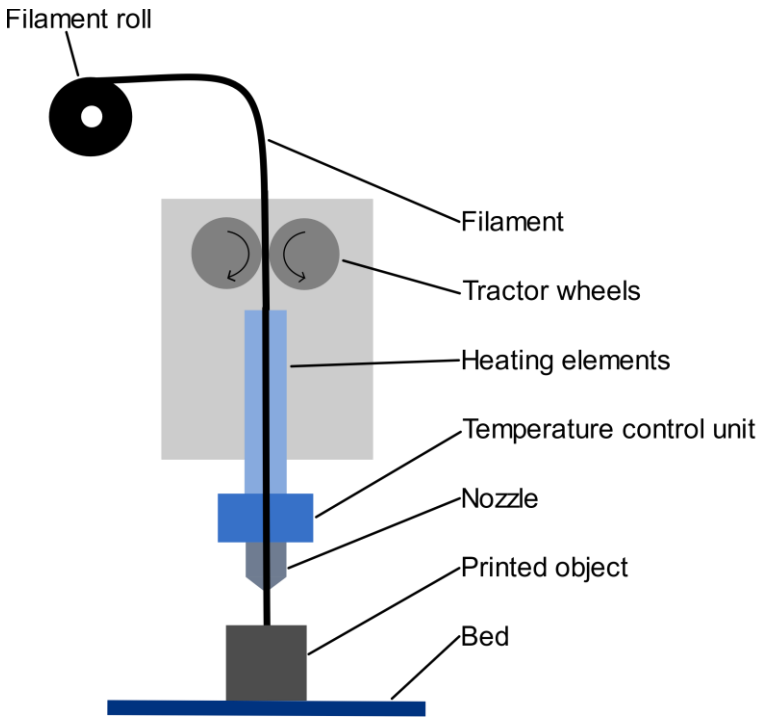

Figure 5. *A schematic presentation of FDM process*

5.1 3D printing parameters affecting surface quality and empty space of the object

Currently, it is difficult to predict the overall accuracy of FDM technique because the process is involved with numerous heavily independent variables. If one parameter is changed, several other parameters are changed simultaneously. This makes it difficult to predict the behaviour of the processing parameters and to control the process to obtain good parts. In many reported studies the parameters are analysed to better understand the process of 3D printing. The most crucial parameters in obtaining good quality objects are layer thickness and nozzle temperature. Therefore, these parameters are studied in this thesis. In addition, several other parameters such as printing speed and nozzle diameter have effect on the quality. [36] In Figure 6 is a schematic presentation of different layer thicknesses and how the empty space varies depending on the layer thickness. The empty space is indicated by red circle. Also, the measuring direction of the surface roughness measurement is shown in the picture. The direction is indicated by red arrow.

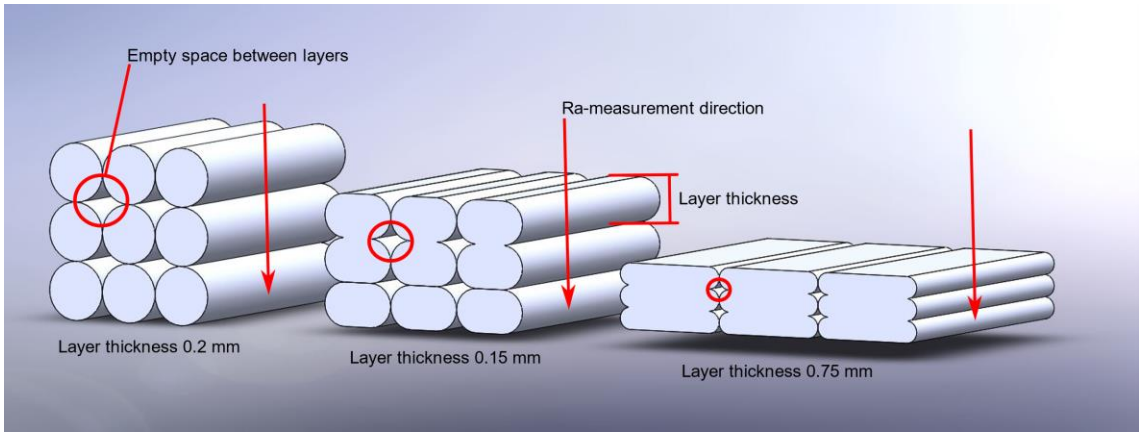

Figure 6. *A schematic presentation of different layer thicknesses*

5.2 Surface roughness of 3D printed objects

As mentioned in Chapter 4, all solid surfaces are rough. The roughness is caused by very fine irregularities which are at very small distances. The measure of the irregularities on the texture of the surface can be determined. Usually, when objects are made by FDM process the surface roughness determination is based on a profile of a perimeter of each layer. [37, 38]

The surface roughness can be indicated by Ra value. As described in the standard ASME B46.1-2019, Ra is “the arithmetic average of the absolute values of the profile

height deviations from the mean line, recorded within the evaluation length" [39]. Ra can be calculated by the following equation

$$Ra = \frac{1}{l}\int_0^l |Z(x)|\, dx \quad (6)$$

Where R_a is the surface roughness, l is the evaluation length, $Z(x)$ is the height of the assessed profile at any position x. [40]

However, the value of surface roughness could not be calculated using the equation 6 because the evaluation length was too short in all cases. The measurement was done so that three lines were drawn: the first line at the tip of the surface roughness peaks, the second line one line at the bottom of the valleys of the surface roughness and the third line in the middle of these previous lines. Then the distance between the first line and the middle line was measured. In Figure 7 is a schematic presentation of how the measurement was conducted.

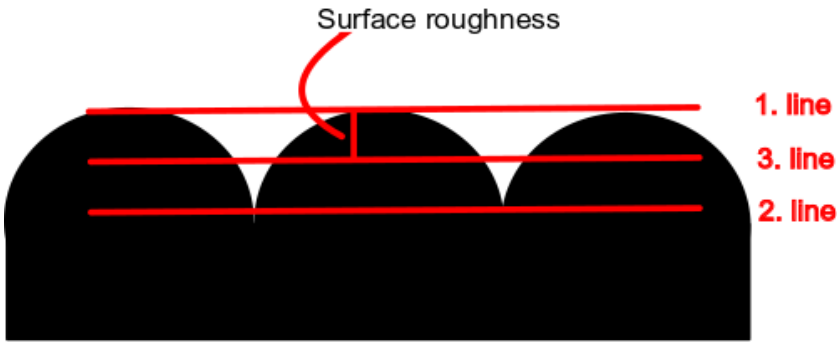

Figure 7. *A schematic presentation of the surface roughness measurement*

6. MATERIALS AND METHODS

In this chapter will be discussed the materials used in the 3D printing, the printed objects, the resistivity measurement and the microscope analysis of the printed objects.

6.1 Filaments used in this thesis

Two different types of filament were used in this study. They both are ABS-based filaments: the matrix of these materials is ABS. ABS is an abbreviation of the words acrylonitrile, butadiene, and styrene. ABS is a terpolymer composed of those three monomers: chemical and thermal stability is provided by acrylonitrile, toughness and strength are increased by butadiene, and shiny finish is given by styrene. ABS is a common amorphous thermoplastic polymer. It is an impact-resistant and opaque engineering thermoplastic. ABS has broad processing window and low melting temperature, making it suitable for 3D printing. ABS is the most widely used material in 3D printing in addition to PLA. The glass transition temperature of ABS is between 95 - 115°C. The temperature range varies depending on the source. [41, 42, 43]

The difference between the two filaments used in this study was that one is conductive and the other permittive. This will be discussed further below.

6.1.1 Conductive filament

The first material which was used in this study was ABS-based conductive filament called Plastic2Print made by Premix Oy. The thickness of the filament is 1.75 mm.

As such, ABS is an insulator like most of the polymers and does not conduct electricity. The volume resistivity of ABS without fillers is > 10.2 Ω·m [44], the volume resistivity of copper is $1.7*10^{-8}$ Ω·m and air 10^{9} to 10^{15} Ω·m [45], respectively. In order for ABS to become electrically conductive, a conductive substance must be added to it. In this study, a filament whose conductivity was obtained by compounding carbon black with ABS was used. The volume resistivity of the filament provided by the manufacturer is 0.25 Ω·m. The filament was custom made and therefore the data sheet is not available.

6.1.2 Permittive filament

The other material used in this study was ABS-based permittive filament called PrePerm® 450 made by Premix Oy. The thickness of the filament is 1.75 mm.

As such, ABS is not permittive. In order to make ABS permittive, inorganic filler with good dielectric properties must be added to it. In this case ceramic filler was used to make ABS permittive. When permittivity is increased using ceramic filler, conductivity is decreased at the same time. Permittivity of the filament is 4.5. The data sheet of the material can be found in Appendix A.

6.2 3D printing

3D printing was done in two phases in the FabLab of Tampere University. The first printings were done in the January 2020 and the second printings in the summer 2020.

6.2.1 The printer

The 3D printer used in this study was Original Prusa i3 MK3S. The Prusa i3 is an open-source 3D printer which is manufactured by Prusa Research. The Prusa i3 MK3 was released in autumn 2017 and it has been improved over the previous models. Some additional improvements have been done to the extruder body and filament sensor of Prusa i3 MK3S and it was released in the beginning of 2019. The Prusa i3 is popular within educators, hobbyists and professionals because of its comparable low price and ease of construction and modification. [46] The diameter of the nozzle of the printer was 0.4 mm in all the printings. In Figure 8 are shown two printers, one inside the box.

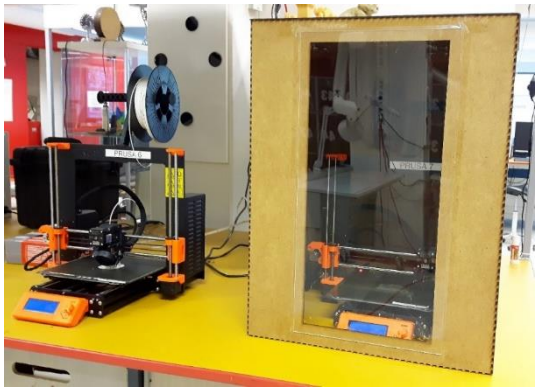

Figure 8. *Two printers, one inside the box*

6.2.2 The printed objects

Two shapes of objects were printed: cube and sphere. The cube was chosen as the geometry because its resistance is relatively easy to measure by compressing it between the electrodes. The size of the cube was chosen to be 2.5 x 2.5 x 2.5 cm because by using that size the effect of the different internal mesh structures can be averaged, and printing would be quite easy, and the material consumption would be relatively small. The size of the cubes with different infill patterns was 1.5 x 1.5 x 1.5 cm. It was chosen for size to optimize both material consumption and printing time. The sphere was chosen as the other geometry because it gives the most regular results in the radar measurement. The radar measurements are obtained from other activities of the project and are not presented in this study. The diameter of the sphere was 3.5 cm.

Both geometries consist of a mesh of equilateral triangles. The mesh structure was created using certain algorithms in MatLab. In cubes marked with “a” the used mesh algorithms are MeshAdapt and Delaunay, in cubes marked with “b” the algorithms are GMSH (A 2D and 3D finite element mesh generator with geometry, meshing and solver modules), MM3G and BAMG (Bidimensional Anisotropic Mesh Generator). In addition, solid objects were printed. In Figure 9 is shown the cut models of the mesh cube and the mesh sphere. The mesh structure inside the objects is clearly seen.

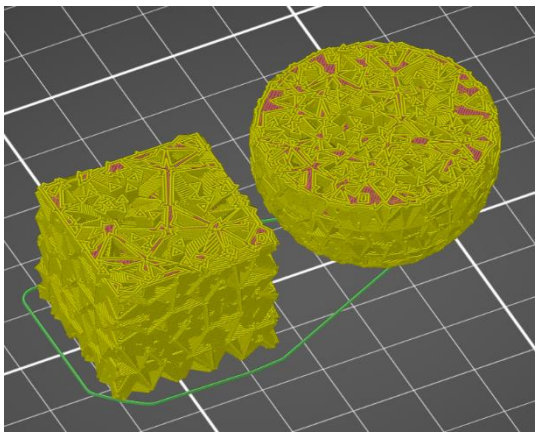

Figure 9. *Cut models of the mesh objects*

Six different sets of objects were printed. In the following Table 3 is also shown which measurements were done for each set.

Table 3. *Measurements made for each set*

		Measurement				
Set	**Mesh/solid**	**Dimen-sions**	**Weight**	**Resistance**	**Surface roughness**	**Empty space/degree of filling**
1st set	Mesh	●	●	●		
	Solid	●	●			
2nd set	Mesh	●	●	●		
	Solid	●	●		●	●
1/3-spheres	Solid					●
Honeycomb				●		
Rectilinear				●		
3D honeycomb				●		

The first set consisted of 12 different mesh cubes and 1 solid cube. The indexing of the cubes is such that the first number indicates the order number of the set: the mesh size is the biggest in the cubes 2 and smallest in the cubes 3. The second number indicates the edge thickness: in each set the mesh size is the same in cubes with the same letter. In the cubes “X.1x” the edge thickness is bigger that in the cubes “X.2x”. The letter indicates the used mesh algorithm as mentioned previously. The indexing and the values for each variable are shown in the Appendix B. The printing parameters were kept constant throughout the printing. The used parameters are in Table 4.

Table 4. *Printing parameters of the 1st set*

Temperature of the filament [°C]	275
Temperature of the bed [°C]	112
Printing speed [%]	100
Fan speed [%]	0

The second set consisted of 4 different mesh cubes and 4 different solid cubes. The mesh structure of the cube 1.1 of the 1st set was used in all the mesh cubes of this set. The indexing of these cubes is such that the last number indicates the thickness of the layer (for example 15 equals to 0.15 mm) and the letter “T” indicates that lower nozzle temperature was used in the printing. The printing parameters of this series varied as shown in Table 5.

Table 5. *Printing parameters of the 2nd set*

	Cube	Nozzle temp. [°C]	Layer height [mm]	Printing time [h:min]
Mesh	10	275	0.10	7:20
	15	275	0.15	4:59
	15_T	255	0.15	5:10
	30	275	0.30	2:14
Solid	10	275	0.10	2:05
	15	275	0.15	1:27
	15_T	255	0.15	1:27
	30	275	0.30	0:42

The indexing of the solid spheres made for microscope analysis is the same as the indexing of the cubes of the 2nd set. Instead of printing whole spheres, only 1/3 of each sphere was printed for microscope analysis to save time and filament. The printing parameters of the spheres are shown in Table 6.

Table 6. *Printing parameters of the 1/3-spheres*

	Sphere	Nozzle temp. [°C]	Layer height [mm]	Printing time [h:min]
Solid	10	275	0.10	1:16
	15	275	0.15	0:48
	15_T	255	0.15	0:48
	30	275	0.30	0:33

Also, three sets of cubes with different infill patterns and infill rates were printed. The set of cubes with honeycomb infill consisted of 5 cubes with different infill rates. The set of cubes with rectilinear infill consisted of 6 cubes with different infill rates and the last set consisted of 5 cubes with different infill rates. The printing parameters for these cubes were the same as the parameters used in printing the 1st set (Table 4). In Figure 10 are shown the different infill patterns with 30 % infill.

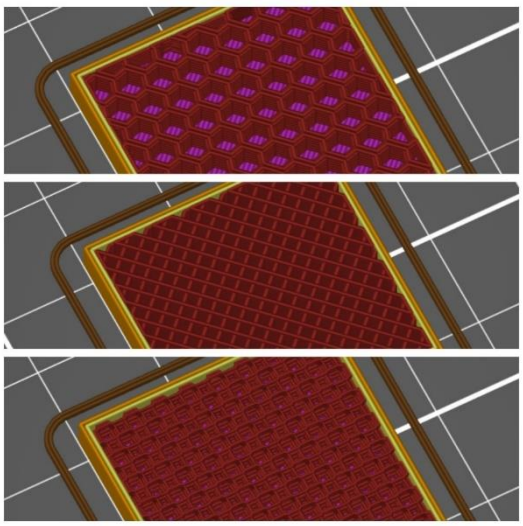

Figure 10. *Different infill patterns. From the top: honeycomb, rectilinear and 3D honeycomb infill*

6.2.3 Problems in printing

Some problems occurred in 3D printing. The problem in the first printings was that the bottom layers of the cube did not stick to the bed of the printer nor each other. To ensure good adhesion between the bottom layers, three raft layers were created under the printed object. After printing, the object was manually removed from the raft layers. Raft layers were not used when the cubes with different infill patterns were printed.

Draught in the FabLab caused a problem. It appeared so that the object was partially separated from the bed. To avoid the effect of the draught, the printer was put into a box, see Figure 6. Also, printers have been used a lot and they were worn out (especially bearings were worn, and belts were stretched) which caused problems. The problems occurred as shifting of the layers. The shifting could also be caused by changes in the printing environment, such as raise in the temperature which could have raised the temperature of the bearings.

Problems in adhesion occurred also in printing the small cubes using different infill patterns and infill percentages. Usually, the infill rate used in most of the 3D printed parts is 20 – 30 %. Especially problematic was to print objects using 3D honeycomb infill with large infill rate (60-90 %). It appeared so that the extrudate did not adhere to the previous layer. Instead, it kept moving along with the nozzle creating a ball of molten filament around the nozzle. Therefore, it was decided to use 10-50 % of infill with 3D honeycomb pattern.

6.3 Optical microscope analysis of the printed objects

The optical microscope (also called a light microscope) is a widely used instrument for examining the structure of an object. It is a very useful and quick tool to check the sample. In a light microscope various lenses are combined together to see the microstructure of the object. A stationary beam of light is reflected off the surface of the specimen, passes through the objective and comprises a magnified image. The image can be captured by a digital camera and processed by computer software. For example, features of the specimen can be measured. [47]

Sample preparation is a crucial part of microscopy examination. It is essential that the sample represents well the entire specimen. In most of the cases it is necessary to first mount the sample to make it easier to handle. There are many ways to carry out the mounting but the most suitable method for polymeric sample is to cast the sample into cold setting thermoset material under vacuum. Also, great care has to be taken in grinding and polishing the sample in order to make the surface of the sample as smooth and scratch-free as possible.

In sample preparation the 3D printed objects were cut horizontally and vertically into samples using Struers Accutom-100 cutting machine. After cutting, the samples were dried in +40°C in a laboratory oven over night. Next day the samples were cast into epoxy under vacuum to make them easier to handle. The used vacuum chamber was Struers CitoVac. When the epoxy was cured the next day, the samples were ground and polished using Struers Tegramin-30 machine. The purpose of this was to make the inner structure of the sample and the possible defects inside the sample more visible. Some of the polished samples are shown in Figure 11. The microscope analysis was done using Leica DM 2500 M light microscope.

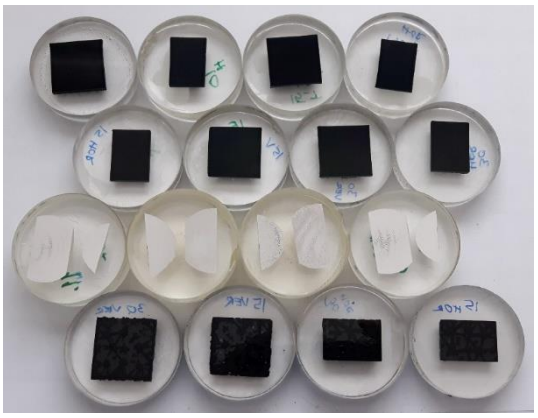

Figure 11. *Some of the polished samples*

Two different types of measurement was used in this study to measure the porosity of the objects: area measurement and line measurement. In the area measurement, pictures were converted to 8-bit images, threshold was adjusted and the percentage of the empty space between the layers in the pictures was calculated using ImageJ 1.53a software.

In the line measurement, the degree of filling of the solid cubes of the 2nd set was calculated from the microscope images in a similar manner. A straight line was drawn across each picture. A 2D graph was plotted in which the intensity varies according to whether the line passes over the layer or the empty space. The data obtained this way was copied to Excel and the degree of filling was calculated.

Both of these measurement techniques indicate basically the same thing but from a slightly different perspective: area measurement indicates the empty space within a certain area and line measurement indicates the degree of filling along the line. This can be seen from Figure 31.

6.4 Resistance measurement method

Because the resistance measurements could not be done according to a standard, another kind of method had to be introduced. It was decided to use a basic method where the measured object is placed between two electrodes and the resistance is measured using a multimeter. In Figure 12 is shown a schematic presentation of the measuring arrangement. The used multimeter was Fluke 175 TRUE RMS Multimeter.

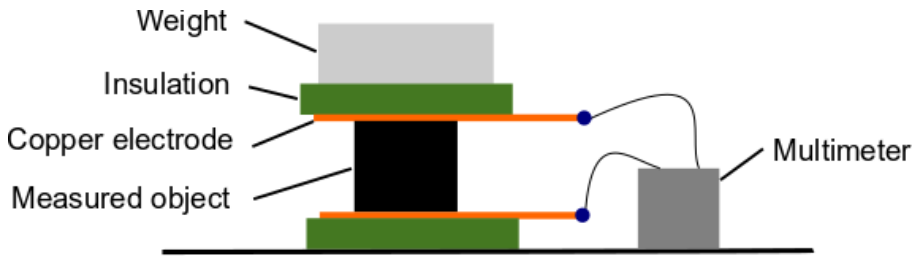

Figure 12. *A schematic presentation of the measuring arrangement*

The most crucial part in developing the method was to find a way to reduce the contact resistance sufficiently. At first, a weight of one kilogram was used on top of the measuring arrangement. The results obtained this way were compared to the rough estimation in which the resistivity of an 3D printed object measured in side-side -direction is less than the resistivity of the filament. The used weight was found too light. Then the weight was increased to 4 kilograms, but it was still too light. In the end, the weight was 8 kilograms, but still it was not enough. After that, a clamp was used to press the electrodes against the measured object. In this way, a sufficient pressure and thus sufficiently low contact resistance was achieved.

The pressure at which the electrodes were pressed against the measured object could not be standardized in this method. In the case of a human being who sets the pressure of the clamp, it is very difficult to set the pressure at the same level every time. An estimate of the amount of the pressure was used and an attempt was made to obtain the same level of the pressure every time. For instance, the clamp was always pressed the same number of times. However, this might be one of the major sources of variation in the results.

It was discovered that the strong pressure caused by the clamp bent slightly the electrodes of thickness 0.3 mm made of soft copper. Electrodes with a thickness of 0.5 mm were tested. Using these thicker electrodes, the resistance increased. It was decided to use the electrodes of thickness 0.3 mm.

It was also observed that the use of an electrode gel significantly reduces the contact resistance. For example, the average resistance of the sample 2.1a using thick electrodes and 4 kg weight without gel is 126.1 kΩ and with gel 59.7 kΩ (all the results are in Appendix C). The decrease in the results is significant when using gel. Therefore, it was decided to use the electrode gel in all the measurements. However, the use of the gel was not straightforward. It was necessary to be able to apply just the right amount of

gel to the surface of the object. If too much gel was applied, the excess drained away between the object and the electrode causing a minor error to the results. If too little amount of gel was applied, it dried out too quickly and again an error was caused. The problem was solved by visually evaluating the appropriate amount of gel. The used gel was Spectra 360 Electrode Gel made by Parker.

It is a known fact that the contact area of the measured object has a great effect on the resistance in resistance measurements. The surfaces which are in contact with the electrodes have to be as straight and smooth as possible. The sharp notches of the triangles of the cubes were sand down using fine sandpaper. Because the work was done manually, the surfaces were not exactly straight nor perfectly smooth after the sandpapering. This reduced the amount of the contact area and increased the resistance.

Although the notches were sanded down, any raft layers possibly left in the object were not sandpapered. This caused one possibility of an error and variation in the results. Another possible cause of an error and variation in the results is the positioning of the object in the clamp. The measured object had to be as centred as possible in both directions to ensure even and good pressure on the surfaces. In addition, it is obvious that errors and problems in the printing of the objects are reflected in the results of the resistance measurements.

7. RESULTS

The results of the measurements and analyses are presented in this chapter.

7.1 Dimensional accuracy of the printed objects

The dimensional accuracy of the objects is one indicator whether the printing was successful. The dimensions of the cubes of 1st and 2nd set were measured using a standard measuring gauge. The gauge was not calibrated. A schematic presentation of how the dimensions were measured is shown in Figure 13.

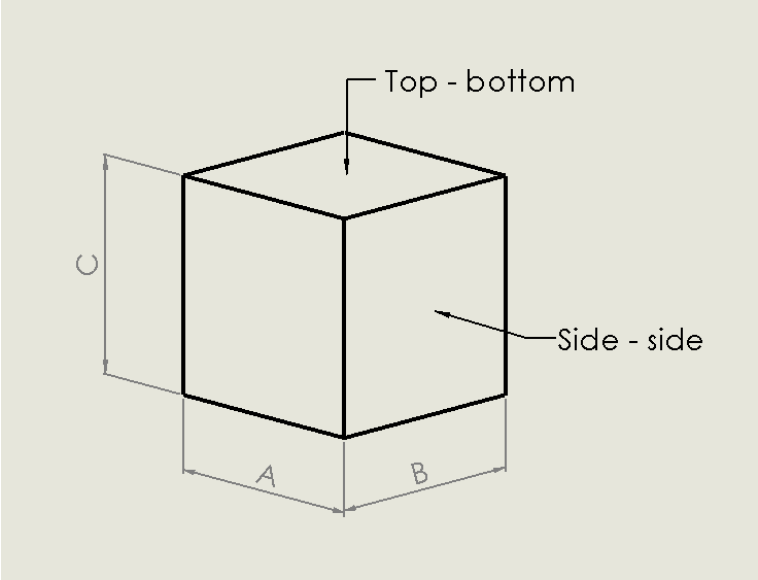

Figure 13. *Measured dimensions of the cubes*

All the results are in Appendix D. The average value of the measurements was taken as a reference value. It was noticed that all the cubes were shrunk more from the bottom than at the top of the object: the measured values of A and B were larger at the top of the object than at the bottom.

The shrinkage of polymers is caused by the difference in the densities of different states (melt and solid). The volume of polymer contracts during cooling. The shrinkage of the objects might be caused by incorrect printing parameters: either too high bed temperature, too high nozzle temperature or incorrect amount of raft layers. If the bed temperature is too high, the polymeric material will have more time to shrink before it cools down and therefore it shrinks more from the bottom than at the top when high temperature is

used. The same phenomenon might happen at the corners of the object with more material than elsewhere. Also, poor environmental conditions, such as draught or wrong ambient temperature might cause shrinkage. The shrinkage might also be related to the material. In general, ABS-based material tends to shrink more than PLA-based, for example. Also, ABS-based material tends to shrink more at the bottom than PLA-based when FDM is used.

In addition, the weight of the objects of the 1st and 2nd set was measured, and the results are shown in Appendix D. A graph was plotted, and linear regression line was drawn to better see the variation in the results of the 1st set. The graph can be seen in Figure 14. It shows the weight of the objects as a function of the edge thickness of the triangles.

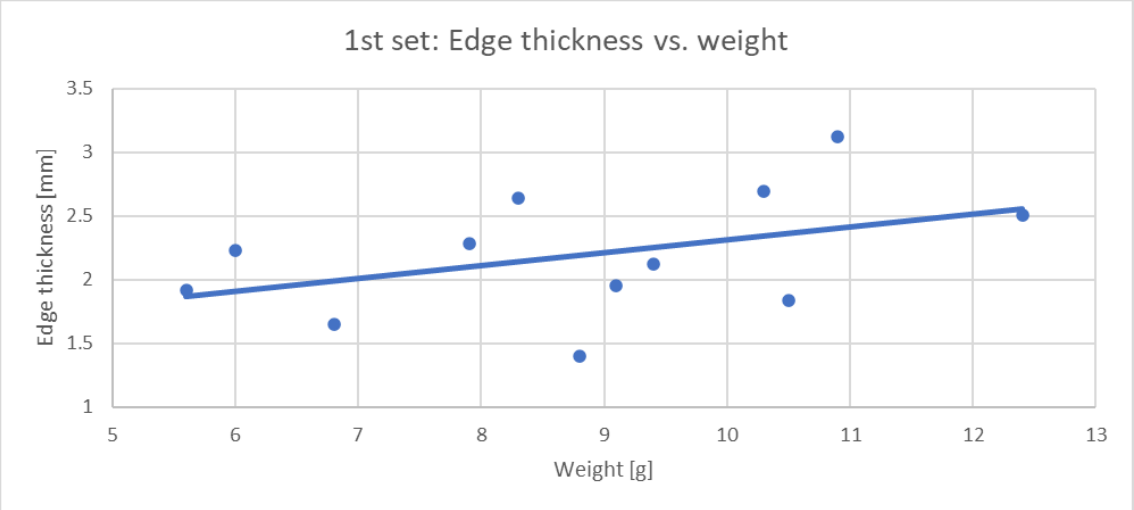

Figure 14. *Weight and edge thickness of the objects of the 1st set*

It can be seen from Figure 13, that the tendency of the weights of the objects correlates well with the edge thickness: as the thickness of the edge increases, so does the weight. Also, a graph of the weighing results of the 2nd set was plotted and it can be seen as Figure 15.

Figure 15. *Weights of the objects of the 2nd set*

Overall, it can be seen from Figure 15 that the weight of the mesh cubes is less than the weight of the solid cubes. Also, in solid cubes the weight increases as the layer thickness increases. This does not happen when the nozzle temperature decreases in the object marked with "T". The opposite phenomenon occurs in the mesh cubes: the weight decreases as the layer thickness increases, excluding in the cube "T", where the nozzle temperature is decreased.

7.2 Microscope analysis

The microscope analysis was carried out using Leica DM 2500 M optical microscope in the laboratory of the Faculty of Materials Science of Tampere University in July 2020. The results are presented in the following chapters.

7.2.1 Surface quality of the printed object

With the naked eye, it can be seen that as the layer thickness increases, the surface roughness increases. In order to obtain comparable numerical results, the variation in surface roughness of the solid cubes of the 2nd set was measured from a microscope image. The measurement was done only in top-bottom direction (z-direction) which is perpendicular to the building direction of the object. In side-side direction (x/y) the surface was so smooth that no differences were observed between the objects. The examples of the microscope images are shown in Figure 16 and the images are in Appendix E. All the images were taken using the same magnification although the scale bars are not visible. The summary of the results is shown in Figure 17 and all the results are in Appendix E.

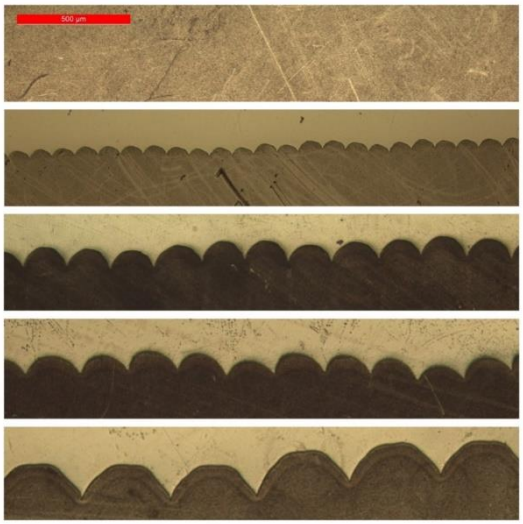

Figure 16. *Examples of the microscope images from the top: scale bar, 10, 15, 15_T and 30*

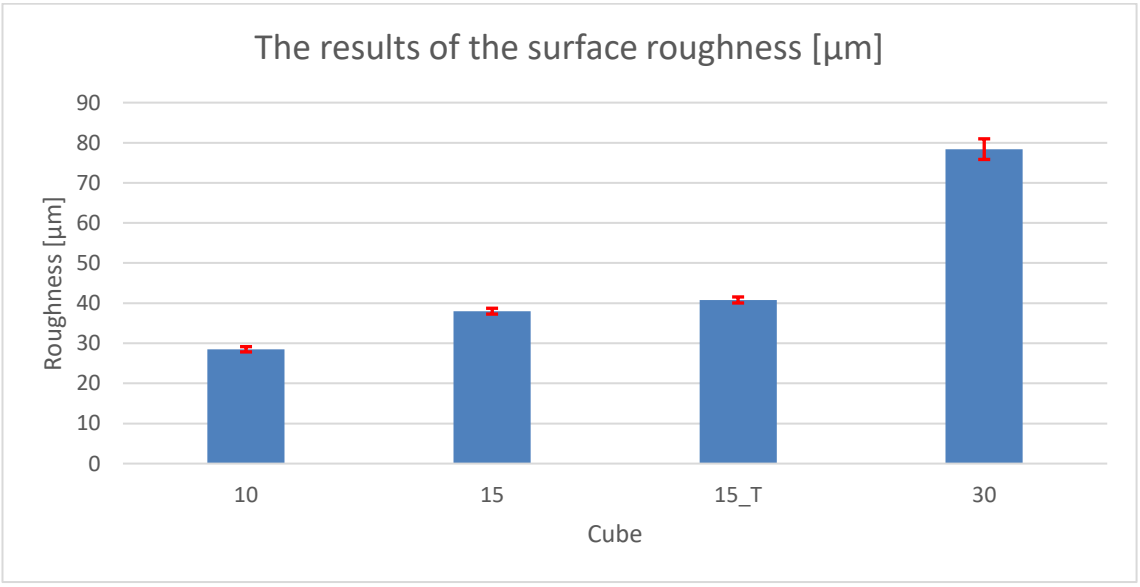

Figure 17. *The results of surface roughness*

From the results of the surface roughness measurements of the solid cubes in Figure 17 can be seen that as the layer thickness increase, the surface roughness increases likewise. This correlates well to the fact that surface roughness increases when using larger layer thickness in 3D printing. The increase in surface roughness when compared 15 and 15_T is due to the waviness of the surface of the sample 15_T. There is no waviness in the sample 15. The red bars in Figure 17 indicate the standard deviation. It can be

seen that the largest standard deviation is in the results of the cube 30. In general, the standard deviation of the results is small.

7.2.2 Porosity and defects inside the printed object

The solid cubes of the 2nd set, and the solid spheres made for microscope inspection were examined using light microscope. Pictures were taken using the Leica Application Suite software. Two different types of measurement was used: area measurement and line measurement. The area measurement was done to both cubes and spheres, the line measurement only to cubes.

The examples of the microscope images are shown in Figures 18 and 21, and the results of the empty space measurement are in Figures 19 and 22, and the results of the degree of filling measurement are in Figure 20. All the pictures seen in Figures 18 and 21 are taken using the same magnification and are presented in Appendixes F and G. The pictures of the solid cubes are presented with the line of the degree of filling calculation and the 2D plot. All the results are presented in Appendix H.

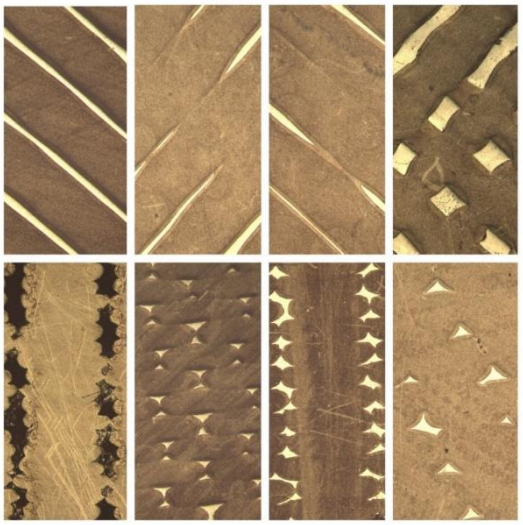

Figure 18. *Microscope image examples of the solid cubes of the 2nd set. Top row: top-bottom view (horizontal cut), from left 10, 15, 15_T and 30. Bottom row: side-side view (vertical cut), from left 10, 15, 15_T and 30.*

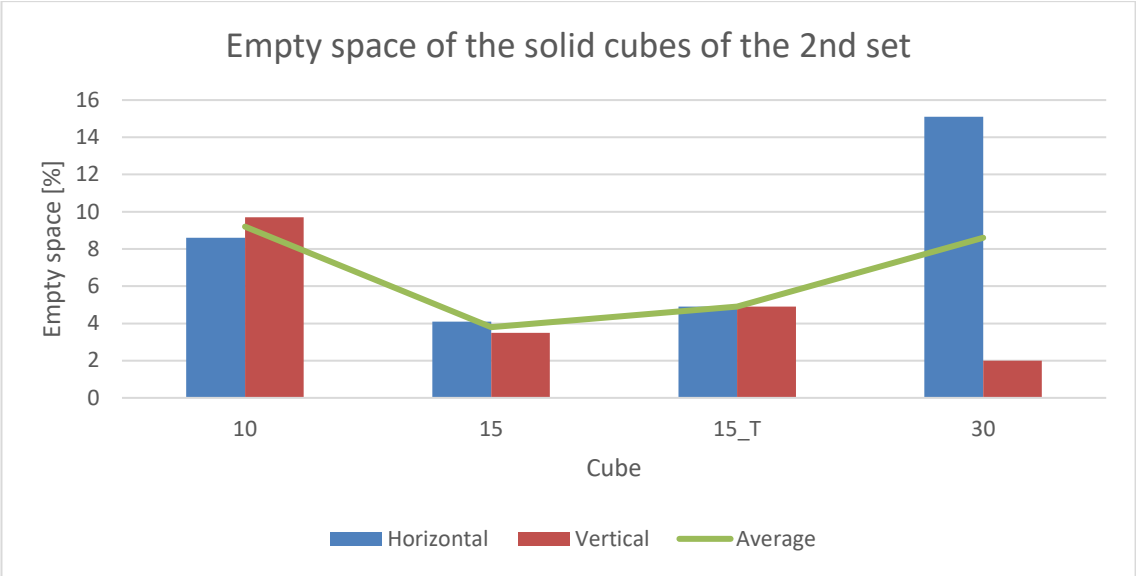

Figure 19. *Empty space of the solid cubes of the 2nd set*

It can be seen from the results in Figure 19 that the largest average amount of empty space between the layers is in the cube 10 and the smallest amount in the cube 15. Based on these results, it can be concluded that the optimal layer thickness for the used nozzle is 0.15 mm. The layer thickness of 0.10 mm is too thin because using that thickness too much empty space appears between the layers. The layer thickness of 0.30 mm is too thick because of the empty space between the layers in top-bottom direction. That is caused by the fact that when the layer thickness increases, the width of the layer decreases in the middle section of the object when the printing volumetric pressure is kept constant. The difference of the empty space in the cubes 15 and 15_T is most likely caused by the decrease in the nozzle temperature: in the cube 15_T the nozzle temperature is lower, and thus the adhesion between the layers is worse and more empty space appears between the layers. Examination of the images did not reveal any porosity in the extrudate. In Figure 20 is shown the degree of filling of the solid cubes of the 2nd set.

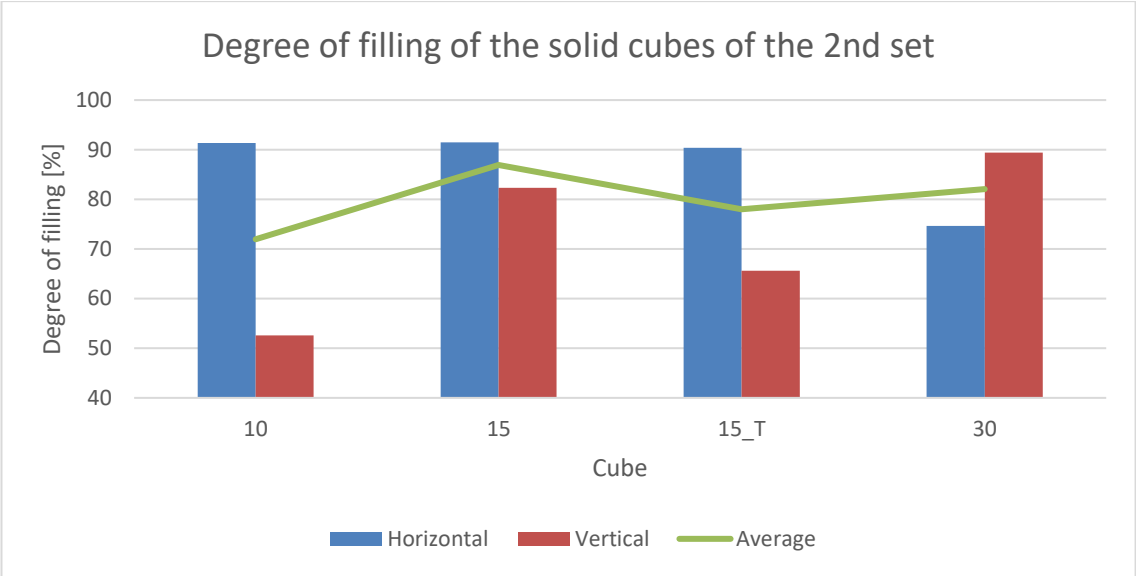

Figure 20. *Degree of filling of the solid cubes of the 2nd set*

In addition, from the results of the degree of filling of the solid cubes of the 2nd set in Figure 20 can be seen that the cube 15 has the highest degree of filling and the cube 10 has the lowest degree of filling. This correlates well with the amount of the empty space in the cube. Based on these results also it can be concluded that the optimal layer thickness for the used nozzle is 0.15 mm, and 0.10 mm is too thin because of the lowest degree of filling.

Extreme caution must be taken when making conclusions based on these results, because the cross-sections are taken from only two points of the sample and the images show only a small fraction of the internal structure of the object.

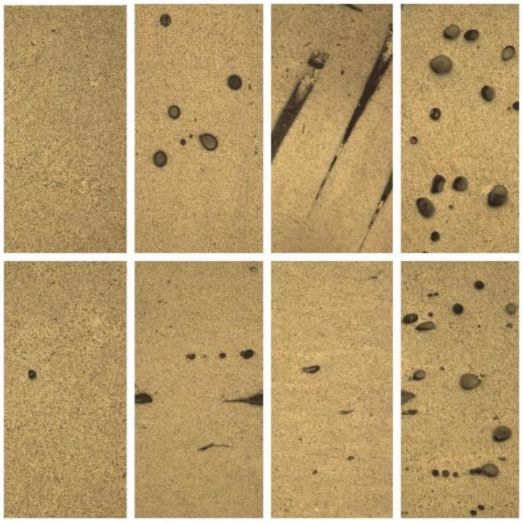

Figure 21. *Microscope image examples of the solid spheres. Top row: top-bottom view (horizontal cut), from left solid_10, solid_15, solid_15_T and solid_30. Bottom row: side-side view (vertical cut), from left solid_10, solid_15, solid_15_T and solid_30.*

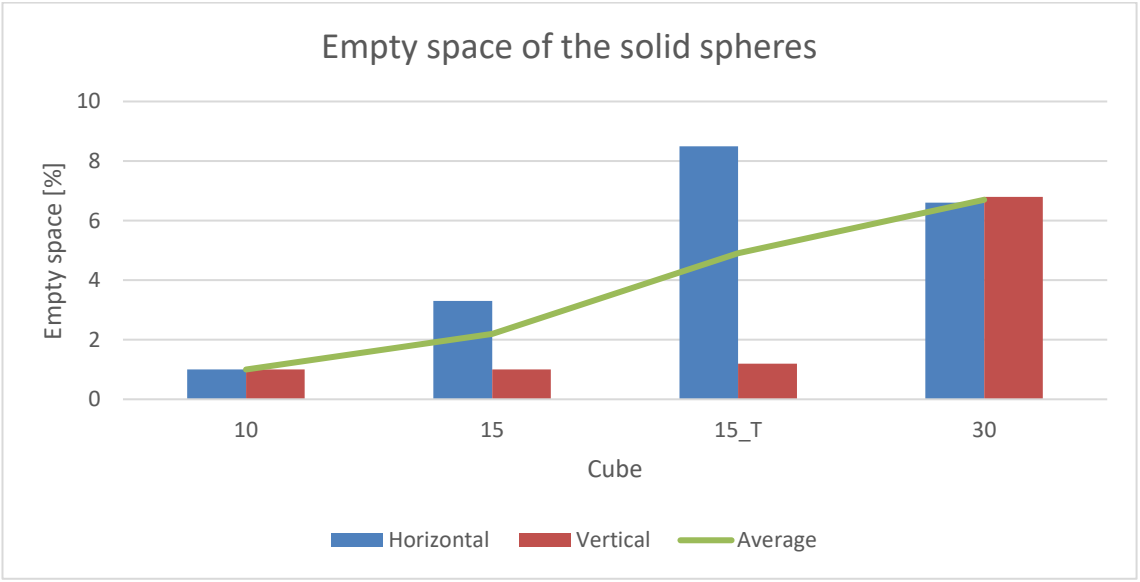

Figure 22. *Empty space of the solid spheres*

The results of the solid spheres in Figure 22 show that the smallest amount of empty space is in the sphere 10, which is almost completely solid (both horizontal and vertical cross-cut looked very similar), and the largest amount of empty space is in the sphere 30. This might be caused by the increase in the layer thickness: the larger the layer thickness, the more space there is inside the printed object. Also, the fact that when using thicker layer thickness, tiny gaps will be harder to fill can be applied to this. The

difference between the spheres 15 and 15_T in top-bottom direction (z-direction, horizontal cut) is due to the difference in the nozzle temperature: using lower nozzle temperature the adhesion between the layers is worse and thus more space appears between the layers. The amount of empty space in the solid spheres correlates well with the results of the radar measurements obtained from other activities of the project and are not presented in this study. Examination of the images did not reveal any porosity in the extrudate.

Extreme caution must be taken when making conclusions based on these results, because the cross-sections are taken from only two points of the sample and the images show only a small fraction of the internal structure of the object.

7.3 Resistance measurements

The resistance measurements were conducted in the FabLab of Tampere University on 9.-24.6.2020. The used method is described in the chapter 6.4.

7.3.1 Repeatability of the method

After a suitable means of compression was found, the repeatability of the method was tested. In testing the repeatability both mesh and solid cube were measured 10 times in both directions (top-bottom (z) and side-side (x/y)). The measuring directions are shown in Figure 13. Then average value, standard deviation and coefficient of variation of the results were calculated. The results were compared based on the coefficient of variation. The results of the repeatability testing of the method are shown in Table 7.

Table 7. *Results of the repeatability test expressed as resistance in Ohms*

	Mesh cube (1.2a)		Solid cube	
	Top-bottom [Ω]	**Side-side [Ω]**	**Top-bottom [Ω]**	**Side-side [Ω]**
1	11110	6460	77.4	69.8
2	10730	5790	76.5	69.3
3	12330	7360	75.7	66.7
4	12640	5600	74.6	74.3
5	10350	6170	81.7	73.3
6	10400	7240	85.1	73.9
7	9040	5980	78.3	71.1
8	8300	6090	78.2	75.5
9	8460	6040	84.2	73.5
10	9020	7150	80.1	72.1
Avg.	10238.0	6388.0	79.2	72.0
St. Dev.	1528.4	637.6	3.5	2.7
COV	14.9	10.0	4.5	3.8

It was found that the solid cube measured in side-side direction has the lowest coefficient of variation, and thus the best repeatability. The coefficient of variation of the mesh cube measured in top-bottom direction was the highest. It indicates that the repeatability of the mesh cube measured in top-bottom direction is the worst. This is well in line with the fact that the properties of a 3D printed object are different in top-bottom and side-side directions. This is due to the fact that the layers of the 3D printed object are oriented in the lateral (side-side) direction. Therefore, electric current is easier to pass through layers in lateral direction because it cannot jump from one layer to another in top-bottom direction. Also, the difference between mesh and solid cube is in line with the fact that resistance is higher in mesh structure than in solid structure because the cross-section of the solid structure is bigger: solid structure has more material along which an electric current can flow, and thus the resistivity of solid cubes is lower. In general, the repeatability of the method is sufficient.

7.3.2 Results of the 1st set

The resistance of the objects of the 1st set was measured and the resistivity was calculated according to the equation 5. All the results are in Appendix H. Three graphs were plotted to better see the variation in the results. In Figure 23 are shown resistivity and edge thickness. In Figure 24 is shown resistivity as a function of the edge thickness, and in Figure 25 resistivity as a function of the median of triangle length. Linear regression lines were created for some variables as seen in the graphs.

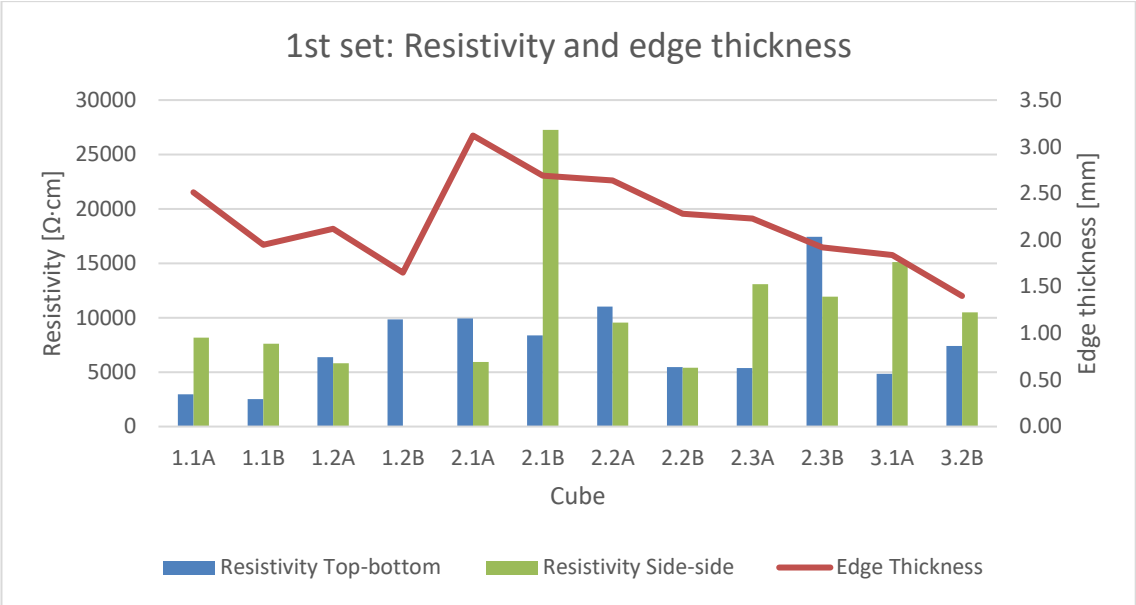

Figure 23. *1st set: Resistivity and edge thickness*

From the graph in Figure 23 can be seen that the resistivity of the cubes 1.2a, 2.1a, 2.2a, 2.2b and 2.3b measured in side-side direction is less than the resistivity measured in top-bottom direction. Furthermore, it can be seen that as the edge thickness decreases within the same subset, the resistivity measured in side-side direction simultaneously decreases in the subsets 1.1, 2.2, 2.3, and in 3.1 and 3.2. This does not happen in the subsets 1.2 and 2.1. The value of the cube 1.2b measured in side-side direction is missing because the cube broke when compressed between the electrodes. The high value of the cube 2.1b measured in side-side direction was most likely due to the cube breaking when compressed between the electrodes or some error in the printing.

The difference in resistivity when measured in different direction is caused by the fact that the properties of a 3D printed object are anisotropic when measured horizontally and vertically. The decrease in resistivity within a subset cannot be caused by the decrease in edge thickness because in theory as the edge thickness decreases, the resistivity increases.

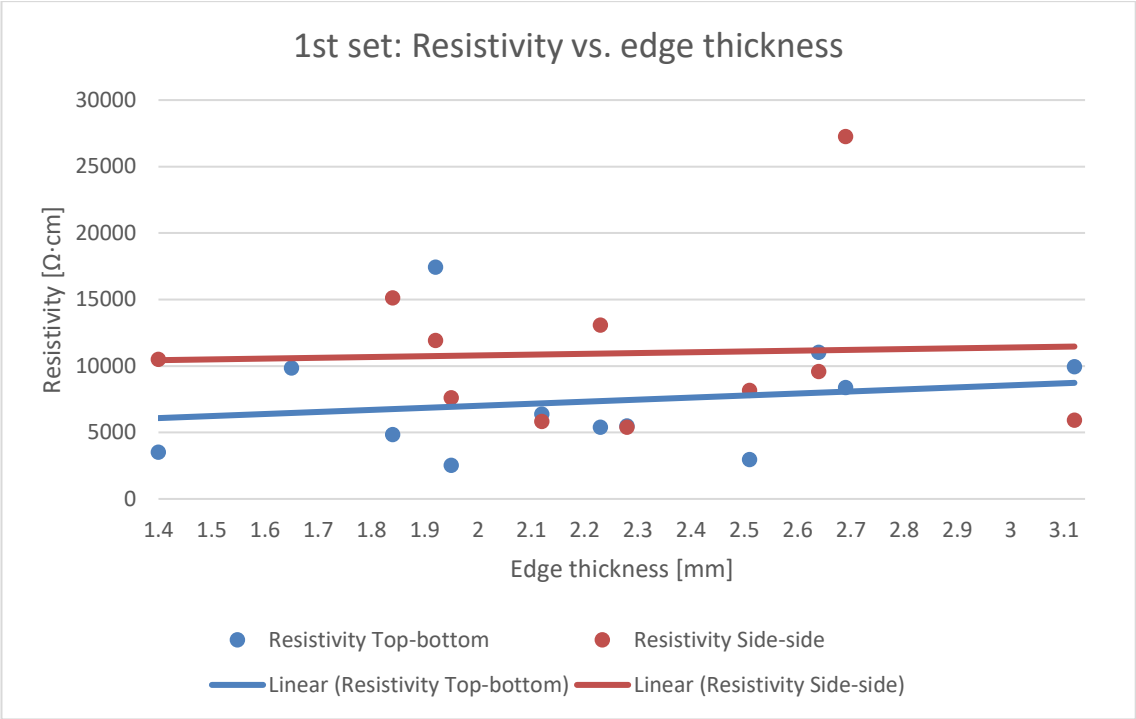

Figure 24. *1st set: Resistivity vs. edge thickness*

It can be seen from the graph in Figure 24 that the resistivity increases as the edge thickness increases when measured in top-bottom direction. When measured in side-side direction the resistivity increases less than measured in top-bottom direction, but it does increases, nonetheless. This might indicate that in the top-bottom direction, the edge thickness has a greater effect on the resistivity than in the side-side direction. In overall, the resistivity level measured in side-side direction is higher than measured in top-bottom direction. One reason for this might be any raft layers possibly left in the object. The raft layers increase the contact surface area in top-bottom direction and thus decrease the resistivity.

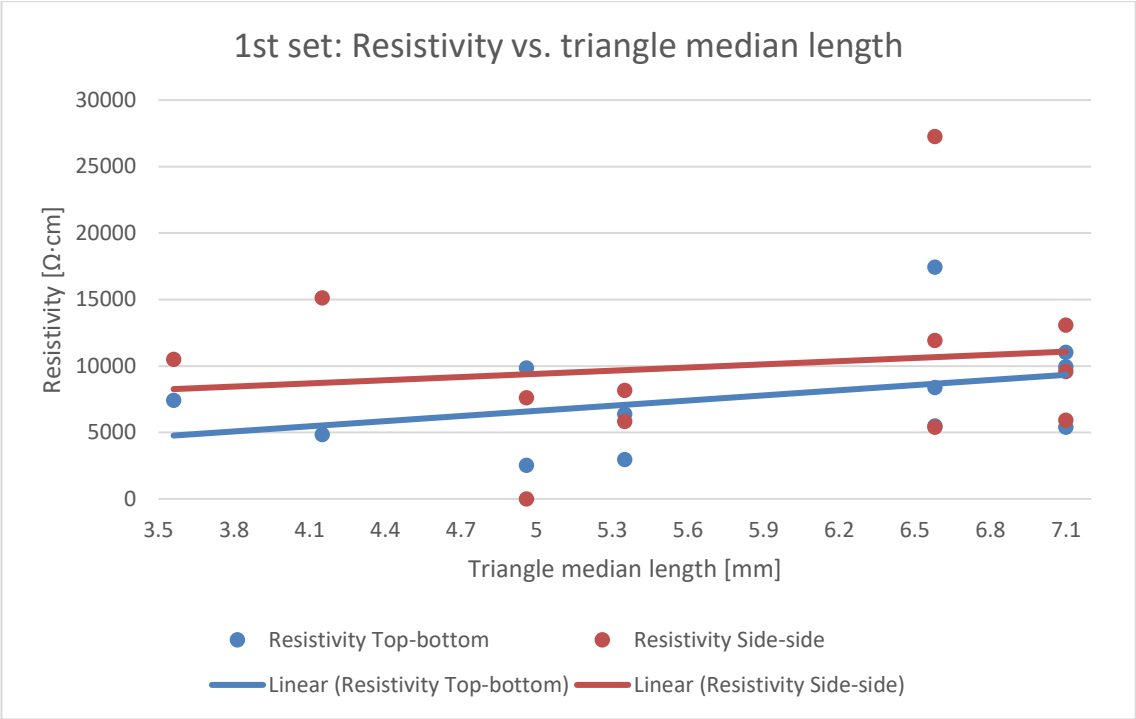

Figure 25. *1st set: Resistivity vs. triangle median length*

It can be seen from the graph in Figure 25 that the resistivity increases as triangle median length increases when measured in top-bottom direction. Resistivity increases when measured in top-bottom direction, but the increase is smaller than in the other direction. This might indicate that the triangle length has greater effect on the resistivity in top-bottom than in the side-side direction. In overall, the resistivity level measured in side-side direction is higher than measured in top-bottom direction. One reason for this might be any raft layers possibly left in the object. The raft layers increase the contact surface area in top-bottom direction and thus decrease the resistivity.

In general, based on these results it can be concluded that both edge thickness and triangle length have effect on the resistivity of the object. In theory, the effect of the edge thickness is the opposite of what these results show: the resistivity should decrease as the edge thickness increases, because when edge thickness decreases the cross section area decreases at the same time and thus the resistivity increases. The possible reasons for the conflicting results are discussed in the following chapter 8.

7.3.3 Results of the 2nd set

The resistance of the objects of the 2nd set was measured and the resistivity was calculated using to the equation 5. All the results are in Appendix I. Graphs were plotted to

better see the variation in the results. In Figure 26 the resistivity is expressed as a function of the layer thickness measured in top-bottom direction. In Figure 27 the resistivity is expressed as a function of the layer thickness measured in side-side direction. Linear regression lines were created for each cube type and measured direction as seen in the graphs. In Figure 28 is shown the effect of the nozzle temperature to the resistivity.

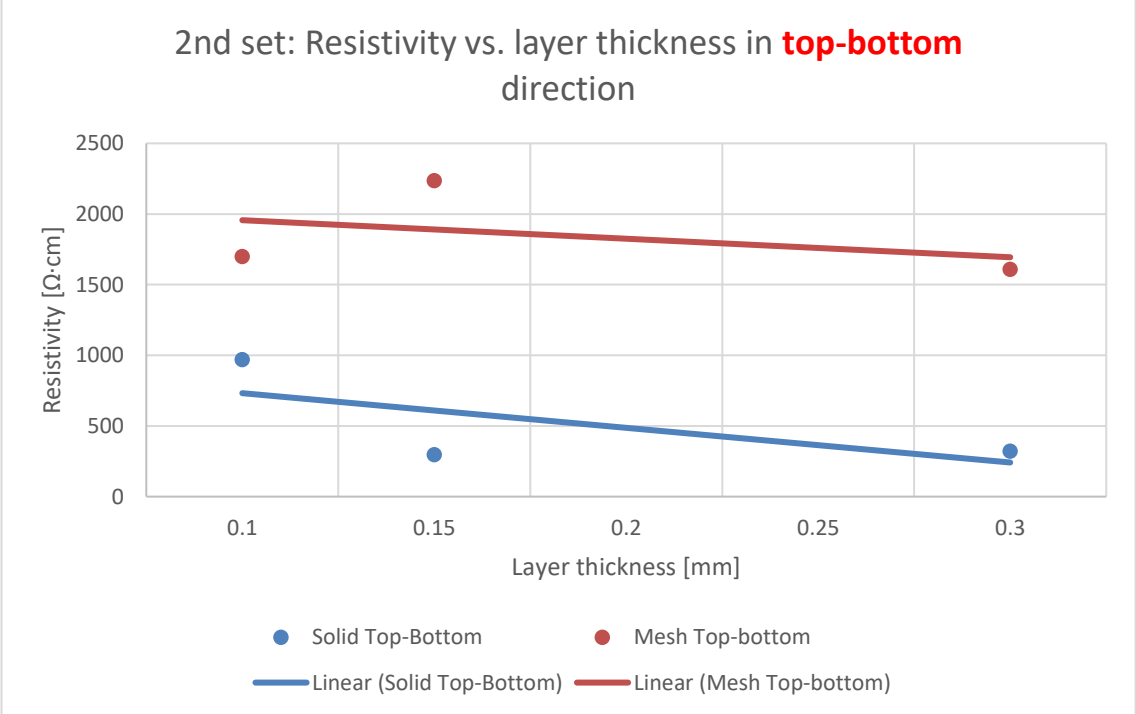

Figure 26. *2nd set: The effect of layer thickness on resistivity measured in top-bottom direction*

It can be seen from the graph in Figure 26 that the level of resistivity of the solid cubes is lower than the resistivity level of the mesh cubes. This is caused by the fact that the cross section area of the solid cubes is larger than the cross section area of the mesh cubes. Furthermore, the resistivity level of the solid cubes decreases a little bit more than the resistivity level of the mesh cubes. This indicates that the layer thickness has greater effect in solid cubes than in mesh cubes. However, the tendency in all the cubes is correct: the resistivity decreases as the layer thickness increases.

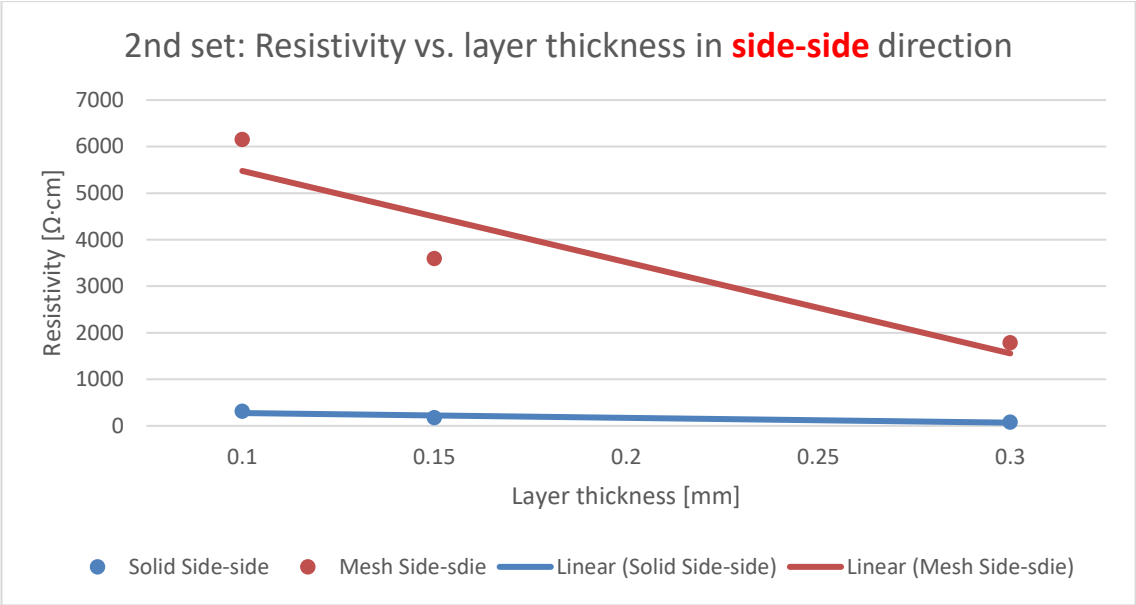

Figure 27. *2nd set: The effect of layer thickness on resistivity measured in side-side direction*

It can be seen from graph Figure 27 that in both solid and mesh cubes, the resistivity decreases as the layer thickness increases. In mesh cubes, the decrease is bigger than in the solid cubes. Therefore, it can be said that the effect of the layer thickness is bigger in mesh cubes. Also, in this case the tendency in all the cubes is correct: the resistivity decreases as the layer thickness increases.

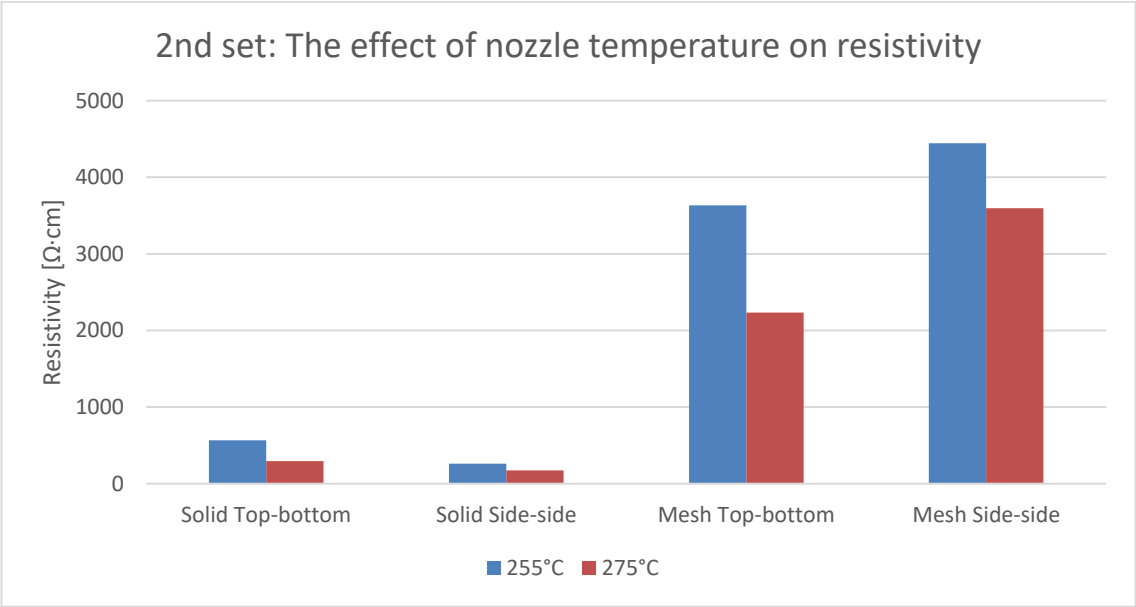

Figure 28. *2nd set: The effect of nozzle temperature on resistivity*

It can be seen from the graph in Figure 28 that the resistivity increases as the nozzle temperature decreases in all the cases. This indicates that the adhesion between the layers in the cube printed using higher nozzle temperature is better than in the cubes printed using lower temperature. The effect of the decrease in temperature is bigger in the mesh cubes than in the solid cubes. This is due to the small features of the mesh cubes: the smaller the features and lower the temperature, the higher the resistivity.

In general, it can be concluded from the obtained results that the resistivity of the solid cubes is lower than the resistivity of the mesh cubes. This is because the cross section area of solid cubes is larger: solid cubes have more material along which an electric current can flow, and thus the resistivity of solid cubes is lower. The change in resistivity in the cubes printed using lower nozzle temperature is most likely due to the fact that cubes printed using lower nozzle temperature have poorer adhesion between the layers. This reduces the contact surface area between the layers and impairs the flow of the electrical current and thus increases the resistivity. In addition, the decrease in the resistivity when going from thinner layer thickness to thicker is due to the increase in the cross-sectional area of the layer: the thicker the layer the larger the cross section area. There are more conducting paths in a larger cross-sectional area, and thus the resistivity is lower.

7.3.4 Results of the cubes with different infill patterns

The resistance of the objects with different infill rates and patterns was measured and the resistivity was calculated according to the equation shown in Chapter 5. All the results are in Appendix J. Two graphs were plotted to better see the variation in the results. In Figure 29 the resistivity is expressed as a function of the infill rate measured in top-bottom direction and in Figure 30 measured in side-side direction. Linear regression lines were created for each infill pattern as seen in the graphs.

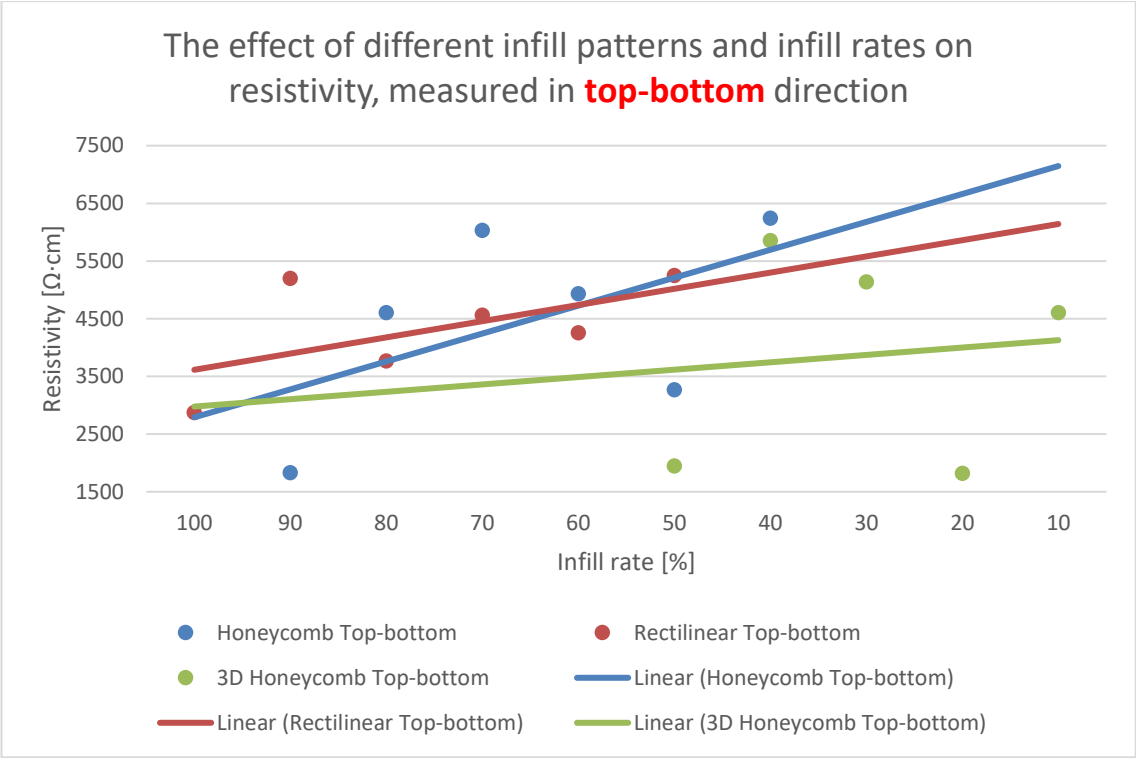

Figure 29. *The effect of different infill patterns and infill rates on resistivity, measured in top-bottom direction*

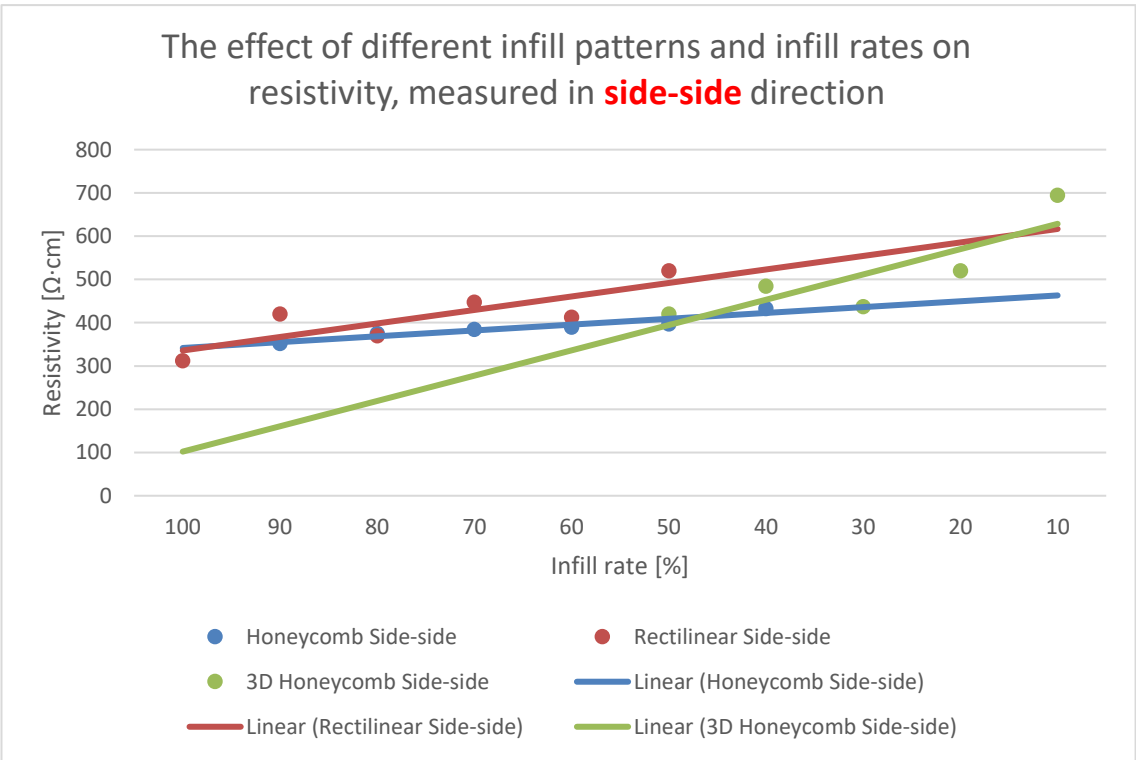

Figure 30. *The effect of different infill patterns and infill rates on resistivity, measured in side-side direction*

It can be seen from the graphs in Figure 29 and 30 that in all cases the resistivity increases as the infill rate decreases. The largest increase in resistivity occurs in the cubes with honeycomb infill measured in top-bottom direction and the smallest in the cubes with honeycomb infill measured in side-side direction. In general, the resistivity level measured in side-side direction is lower than measured in top-bottom direction. This is due to the fact that the properties of a 3D printed object are anisotropic when measured horizontally and vertically. Typically, the resistivity is lower in side-side direction which is the same direction as the layers are oriented.

The variation in the results measured in side-side direction is smaller than in the results measured in top-bottom direction. This is due to the fact that the layers of the 3D printed object are oriented in the lateral (side-side) direction. Therefore, electric current is easier to pass through layers in lateral direction because it cannot jump from one layer to another in top-bottom direction. In addition, variation in adhesion between the layers causes variation in the results.

It can be seen that the larger the infill rate, the larger the cross-sectional area through which electricity can flow. The larger the cross-sectional area, the lower the resistivity. The greatest effect of the degree of infill is in the honeycomb structure.

7.4 Empty space and filling degree vs resistivity of the 2nd set solid cubes

The results of the empty space and filling degree measurements of the solid cubes of the 2nd set were compared to the results of the resistivity measurements of the same samples. In Figure 31 are shown the results. The comparison chart is in Appendix L.

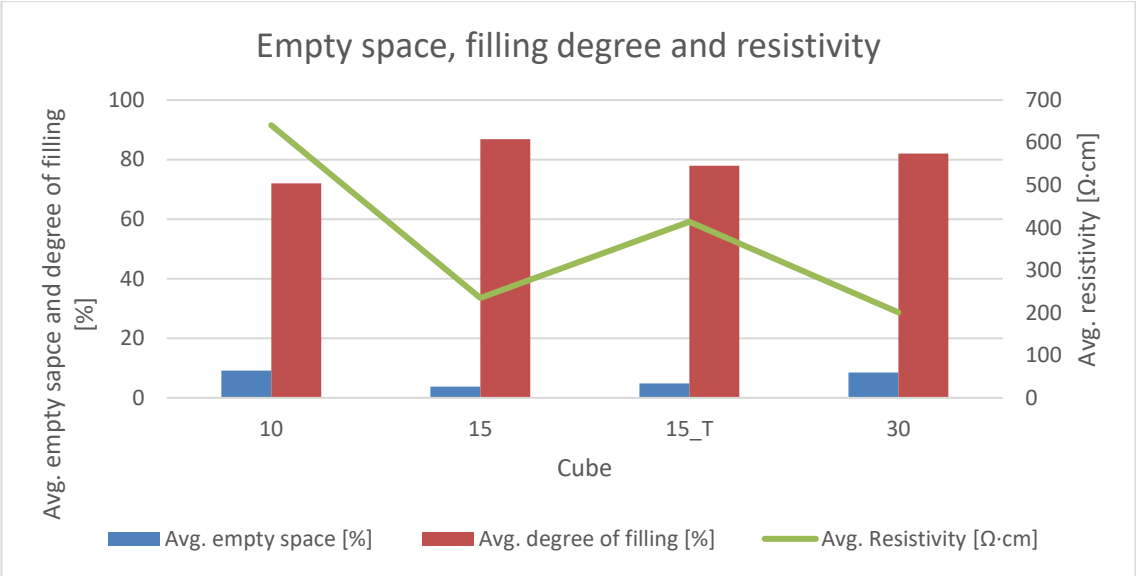

Figure 31. *Average empty space and degree of filling, and average resistivity of the solid cubes of the 2nd set*

From the results in Figure 31 can be seen that the cube 10 has the highest amount of empty space, the lowest degree of filling and thus the highest average resistivity. This in line with the facts. The cube 15 has the lowest amount of empty space and the lowest degree of filling but it does not have the lowest resistivity. The cube 30 has the lowest resistivity most likely because its amount of empty space in vertical direction is as low as 2.0 % and the resistivity measured in the same direction only 82 Ω·cm. In overall, the degree of filling correlates quite well with the resistivity: as the degree of filling increases, the resistivity decreases.

However, there are more factors than empty space and degree of filling that have effect on resistivity. Also, adhesion between the layers, and the inner structure of both the object and the extrudate have effect on the resistivity.

7.5 Permittivity calculations

Permittivity of the solid spheres was calculated based on the empty space measurements using the mixing model equation 4 presented in Chapter 3.3. Here, the volume fractions were calculated based on the empty space measurement presented in Appendix H, the complex permittivity of the polymer composite is 4.5 as shown in the data sheet of the material (Appendix A), and the degree of the model is 0.4 [24] because it is a mixture of three components: air, ABS as matrix and ceramic filler. The results of the

calculations are in Appendix M. A graph was plotted to see the variation in the results, it is seen in Figure 32.

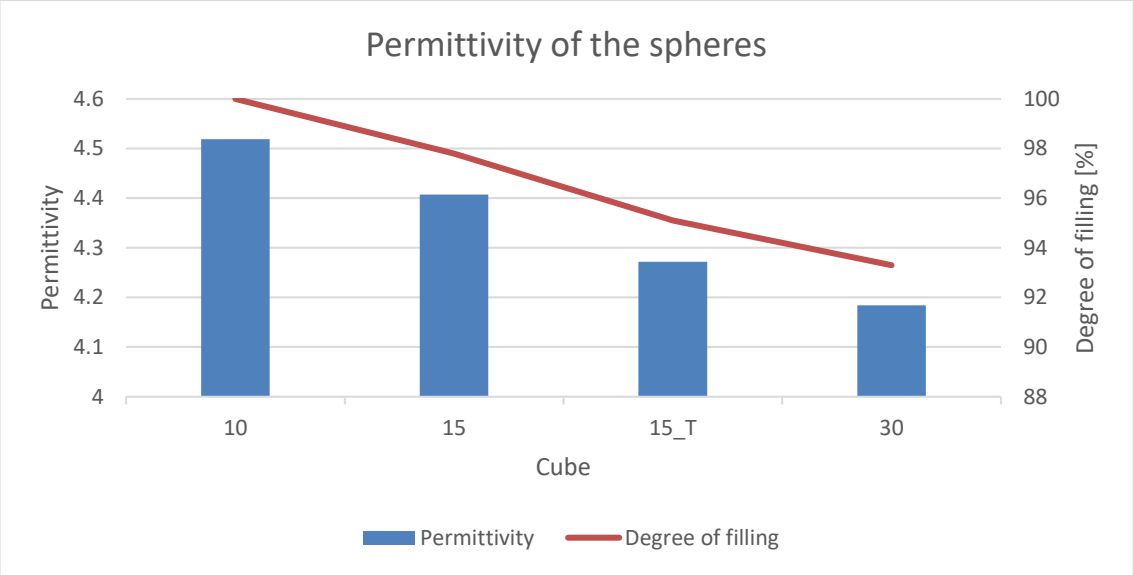

Figure 32. *Permittivity of the spheres*

From Figure 31 can be clearly seen that the permittivity decreases as the degree of filling inside the sphere decreases. That is caused by the fact that the permittivity of air is ~ 1 (1.00059) and the permittivity of the polymer composite is 4.5. The more there is empty space and the less polymer composite in the mixture, the lower is the permittivity.

7.6 Summary of the results

- 3D printing parameters affect the macrostructure of an object.
- The resistivity and permittivity of the object can be affected by varying the 3D printing parameters.
- It was noticed that air and empty space appear in the object: empty space is caused by poor adhesion between the layers or incorrect printing parameters.
- The effect of the 3D printing parameters on the object can be seen in the results of the resistance measurements and the microscope analysis.
- The micro- and macrostructure has a connection, and it is true in the case of conductivity.
- The difference in resistivity between horizontal and vertical direction is true.

8. DISCUSSION

Previous studies have found that the used process parameters and the levels of the parameters affect the performance of the FDM process. A sufficient way to improve the quality of the surface and the printed object is to optimize the process parameters. Previous results indicate that layer height has a significant influence on the surface roughness and the overall quality of the object. Also, printing speed and nozzle temperature have effect on the surface roughness, but their effect is not entirely clear. Infill rate and nozzle diameter have effect on the porosity of a 3D printed object. [48, 49]

The effects of FDM parameters on the surface roughness of an object have been the subject of many studies. These studies show that the layer thickness is the main factor influencing the surface roughness. It was also found that there is an inverse relation between layer thickness and surface roughness. [50, 51] Nancharaiah et. al. found in their study that the surface quality of the printed object is improved by lower layer thickness. [52] Chaidas et al. have studied the surface roughness of PLA objects made by FDM technique. They found that surface roughness decreases when material melting temperature increases. [53] You also studied the optimization of the printing parameters of an object printed of PLA. He concluded that the surface roughness is directly proportional to the printing speed. [54] In the study of Valerga et. al. the effect of printing speed and temperature of the extruded filament was examined. It was found that when temperature increases the surface quality degrades. It was also found that increase in printing speed enhances the surface quality. [55] In these studies, the roughness of the surface is studied from the printed object point of view.

It was found in this study that the layer thickness has effect on the surface roughness: the higher the layer thickness the larger the surface roughness. This is in line with the results of Nancharaiah et. al. The nozzle temperature affected on the surface roughness so that as the nozzle temperature decreased surface roughness increased because of the waviness of the surface. This result is the opposite with the results of Chaidas et. al. The effect of the printing speed on the objects was not studied in this thesis.

If properties which are affected by the internal structure of the object (resistivity, conductivity, permittivity) are to be studied, it is important to know how the printing parameters affect the internal structure (porosity etc.) of the part. The parameters influencing the

internal structure of the object have not been studied as much as the parameters influencing for example the mechanical properties. Buj-Corral et. al. have studied the influence of infill rate and nozzle diameter on porosity of the object. They found that porosity decreases as the infill rate decreases despite of the nozzle diameter. They also consider using the extrusion multiplier parameter. [48] Dev et. al. have studied the printing parameters from a mechanical point of view. They found that when 80 % infill rate, 0.2 mm layer thickness and gyroid pattern is used, the compressive strength is close to the solid sample. It can be thought that the sample is solid. [56] Gary Hodgson writes in his article that if two adjacent paths are too distant or not enough material is extruded, gaps between the layers will be visible. By changing the ratio between flow speed and head speed the paths can be made thicker or thinner. When using thicker paths, tiny gaps will be harder to fill and when using thinner paths less bonding is provided. [57]

In this study was found that the infill rate has effect on the porosity of the object. In this study the porosity inside the object increased as the infill rate decreased. This can be seen from the results of the cubes with different infill rates and patterns: resistivity increases as the infill rate decreases. This tells that the lower the infill rate the more porosity inside the object and higher the resistivity. This result does not correlate with the results of Buj-Corral et. al. This study also showed that the layer thickness effects the porosity inside the object, and it is in line with the article of Hodgson.

This study began by creating objects with different mesh structures, layer thicknesses and triangle sizes in MatLab. Also, solid objects with different layer thicknesses were created. The objects were then 3D printed by FDM. After that the resistance of the objects was measured, resistivity calculated, and the inner structure of the objects examined by optical microscope. During the research process, several points have emerged that affect the comparability and reliability of the results.

It was found that a mesh structure crated using MatLab can be used to model and adjust permittivity and resistivity of an object. However, the mesh structure used in this study proved to be too complex and consisted of too small features. The mesh structure was difficult to execute using 3D printer and the adhesion between the layers of the small features was poor. This can be seen in the results of the resistance measurements and also in the microscope images. On the other hand, the resistivity of the solid objects can be predicted.

There are also many sources of error in the FDM process. The printers used in this study were much used and worn out. The calibration of the printers was done manually and visually by different users. This will no doubt cause some inaccuracy in the printing process and the objects. Shrinking of the printed objects might indicate that the printing parameters were incorrect, although it can be material related issue as well. Incorrectly set parameters may, at worst, cause the conductive paths to be broken, but this is highly unlikely. Broken conductive paths affect conductivity and resistivity. Also, it is difficult to see the errors inside the objects without breaking them and therefore it is difficult to adjust the printing parameters. Even if the infill rate of the settings is 100 %, the object is still not completely solid because the final infill rate is affected by many other parameters than only the infill rate, such as the nozzle diameter, layer thickness and extruder multiplier. There are also many possibilities for errors in the resistance measurement method. They are discussed in the chapter 7.4.

A good way to determine how successful the printing has been is to compare the weight of the STL-model and the weight of the printed object. In this study, the object could not be detached from the raft layers with sufficient accuracy, and some of the raft layers remained in the object. Therefore, the comparison between the weights could not be done.

Both the amount of empty space inside the object and the degree of filling of the object have effect on the resistivity of the object: the less there is material inside the object and more air and empty space, the higher is the resistivity. It is because of the known fact that air is a good insulator. Also, the calculated permittivity of the solid spheres correlates well with the amount of the empty space inside the objects.

On the other hand, it was found in this study that the properties of a 3D printed object are anisotropic: resistivity in a 3D printed object is higher in top-bottom (z) direction than in the side-side (x-y) direction. It was also found that the nozzle temperature affects the adhesion between the layers and thus resistivity and permittivity of the object. Also, the layer thickness has effect to the properties: the layer thickness affects the empty space between the layers and the degree of filling and thus resistivity and permittivity.

Based on this study, it can be said that it is possible to predict the resistivity of a solid 3D printed object. Also, the effect of different 3D printing parameters on the porosity of an object is better known. When comparing the obtained resistivity values to the resistivity values of different human tissues can be seen that some of the resistivity values of the

printed objects correspond well to some of the tissue resistivity values. For example, the resistivity on cerebrospinal fluid is 56 Ω·cm and the resistivity of the solid cube 30 of the 2nd set in side-side direction is 82 Ω·cm. Also, the resistivity of grey matter and skin in 303 Ω·cm, and the resistivity of the solid cube 10 of the 2nd set in side-side direction is 313 Ω·cm, and the resistivity of the solid cube 15 of the 2nd set in top-bottom direction is 295 Ω·cm.

Table 8. *Comparison table of the results and different human tissues*

	Resistivity [Ω·cm]
Cerebrospinal fluid	*56*
Solid cube 30 of 2nd set, side-side	82
Grey matter	*303*
Skin	*303*
Solid cube 10 of 2nd set, side-side	313
Solid Cube 15, of 2nd set, top-bottom	295

9. CONCLUSIONS

The objective of this thesis was to study how the structure effects to resistivity and permittivity of a 3D printed analogue object. This was done by creating analogue objects using certain algorithms, printing the objects using FDM method and analysing their electromagnetic properties. Also, the inner structure of the objects was examined, and permittivity was calculated. A lot has been learned about different 3D printing parameters and their effect on the printed object. Also, the essential parts of the resistance measurement of 3D printed objects are now known.

It was found in this study that the inner structure of the object have effect on the electromagnetic properties such as resistivity and permittivity: the resistivity of the mesh structure is higher than the resistivity of the solid structure. The inner structure of the object can be controlled by FDM parameters: the layer thickness of the object effects the empty space inside the object. It was also found that the properties of a 3D printed object are anisotropic.

Further studies are needed to improve the design of the mesh structure of the cubes to make it simpler. Also, resistance measurement system has to be improved to make it more accurate and reliable. Optimization of the 3D printing parameters is essential to improve the quality of the printed objects and to ensure the precise inner structure of the objects. The effect of the extrusion multiplier function on the objects and their quality is worth to study.

REFERENCES

[1] Denisov, A. M. Elements of the Theory of Inverse Problems. De Gruyter, Utrecht, the Netherlands. p. 1. 1999.

[2] Wolters, C. H. et. al. Influence of Tissue Conductivity Anisotropy on EEG/MEG Field and Return Current Computation in a Realistic Head Model: A Simulation and Visualization Study using High-Resolution Finite Element Modeling. NeuroImage. Vol. 30. Iss. 3. p. 813-826. 2006.

[3] Mohammad, S. A. et. al. Surface Roughness Quality and Dimensional Accuracy—A Comprehensive Analysis of 100% Infill Printed Parts Fabricated by a Personal/Desktop Cost-Effective FDM 3D Printer. Materials Science and Applications. No. 9. p. 11-40. 2018.

[4] Eykhoff, P. System Identification-Parameter and State Estimation. John Wiley & Sons. London. 1974.

[5] Sterrett, S. G. Experimentation on Analogue Models. Springer Handbook of Model-Based Science. Springer International Publishing. p. 857-878. 2017.

[6] Mills, N. J. Plastics - Microstructure and Applications (3rd Edition). Elsevier. p. 24-25. 2005.

[7] Santini, Al. Automotive Electricity and Electronics (2nd Edition). Cengage Learning, Inc. p. 18. 2013.

[8] Radzuan, N. A. M. et. al. A review of electrical conductivity models for conductive polymer composites. International Journal of Hydrogen Energy. No. 14. p. 9262-9273. 2017.

[9] Alemour, B. et. al. A Review of Using Conductive Composite Materials in Solving Lightening Strike and Ice Accumulation Problems in Aviation. Journal of Aerospace Technology and Management. No. 11. p. 3. 2019.

[10] Aribou, N. et. al. Prediction of filler/matrix interphase effects on AC and DC electrical properties of carbon reinforced polymer composites. Polymer Composites. Vol. 40. Issue 1. p. 346-352. 2019.

[11] Gulrez, S. et.al. A review on electrically conductive polypropylene and polyethylene. Polymer Composites. Vol 35. p. 900-914. 2014.

[12] Brigandi, P. J. Electrically Conductive Multiphase Polymer Blend Carbon-Based Composites. Theses and Dissertations. Lehigh University. Lehigh Preserve. p. 6. 2017.

[13] Clingerman, M. L. Development and modelling of electrically conductive composite materials. A Dissertation. Michigan Technological University. p. 13. 2001.

[14] Clingerman, M. L. Evaluation of electrical conductivity models for conductive polymer composites. Journal of Applied Polymer Science. No. 83. p. 1341-1356. 2001.

[15] Harito, C. et. al. Polymer Nanocomposites having a High Filler Content: Synthesis, Structures, Properties, and Applications. Nanoscale. The Royal Society of Chemistry. Iss. 11. p. 4653-4682. 2019.

[16] Zhang, W. et. al. Carbon based conductive polymer composites. Journal of Materials Science. p. 3408-3418. May 2007.

[17] Iqbal, A. et. al. The Effect of Filler Concentration on the Electrical, Thermal, and Mechanical Properties of Carbon Particle and Carbon Fiber-Reinforced Poly(styrene-coacrylonitrile) Composites. Polymer Composites; Newtown. Vol. 28. Iss. 2. p. 186-187. 2007.

[18] Engineering Design Handbook - Discontinuous Fiberglass Reinforced Thermoplastics: (DARCOM-P 706-314). U.S. Army Materiel Command. p. 3_16. Retrieved from Knovel 4.6.2020.

[19] Sturdivant, R. Microwave and Millimeter-Wave Electronic Packaging. Artech House. p. 17-18. 2014.

[20] Clavier, R. Characterization and Analysis of Polymers. John Wiley & Sons. p. 55. 2008.

[21] Zhang, C. et. al. Polymer composites with balanced dielectric constant and loss via constructing trilayer architecture. Journal of Materials Science. No. 53. p. 13230–13242. 2018.

[22] Sihvola, A. Mixing Rules with Complex Dielectric Coefficients. Subsurface Sensing Technologies and Applications Vol. 1. No. 4. 2000.

[23] Kärkkäinen, K. K. et. al. Effective Permittivity of Mixtures: Numerical Validation by the FDTD Method. IEEE TRANSACTIONS ON GEOSCIENCE AND REMOTE SENSING. Vol. 38. No. 3. 2000.

[24] Sihvola, A. et. al. Mixing Formulae and Experimental Results for the Dielectric Constant of Snow. Journal of Glaciology. Vol. 31. No. 108. 1985.

[25] Conductive graphene filament. https://www.blackmagic3d.com/. Retrieved 19.8.2020.

[26] Electrifi Conductive Filament. https://www.multi3dllc.com/product/electrifi/. Retrieved 19.8.2020.

[27] Raw materials. https://www.preperm.com/products/raw-materials/#preperm-standard-grades. Retrieved 19.8.2020.

[28] Electrically Conductive Composite PLA. https://www.proto-pasta.com/products/conductive-pla. Retrieved 19.8.2020.

[29] Grellmann, W. et. al. Polymer Testing (2nd Edition). Hanser Publishers. p. 343. 2013.

[30] Slade, P. G. Electrical Contacts, 2nd Edition. CRC Press. p. 1. 2017.

[31] Hamedi, M. et. al. A review of electrical contact resistance modeling in resistance spot welding. Welding in the World. Iss. 61. p. 269-290. 2017.

[32] Electrical resistivity and conductivity. https://en.wikipedia.org/wiki/Electrical_resistivity_and_conductivity. Retrieved 22.8.2020.

[33] Gibson, I. et. al. Additive Manufacturing Technologies 3D Printing, Rapid Prototyping, and Direct Digital Manufacturing. New York, NY: Springer New York: Imprint: Springer. 2nd edition. p. 4-6, 147-165. 2015.

[34] Turner, N. et. al. A review of melt extrusion additive manufacturing processes: 1. Process design and modelling. Rapid Prototyping Journal. Vol. 20. No. 3. p. 192-204. 2014.

[35] Narayan, R. Rapid Prototyping of Biomaterials - Techniques in Additive Manufacturing (2nd Edition). Elsevier. p. 132. 2020.

[36] Abeykoon, C. et. al. Optimization of fused deposition modeling parameters for improved PLA and ABS 3D printed structures. International Journal of Lightweight Materials and Manufacture. Vol. 3. Iss. 3. p. 284-297. 2020.

[37] Choudhury, S. K. et. al. 1.3 Finish Machining of Hardened Steel. Comprehensive Materials Finishing. Elsevier. Vol 1. p. 66-67. 2017.

[38] Taufik, M. et. al. A Study of Build Edge Profile for Prediction of Surface Roughness in Fused Deposition Modeling. Journal of Manufacturing Science and Engineering. ASME. No. 138(6): 061002. 2016.

[39] ASME B46.1-2019. Surface Texture (Surface Roughness, Waviness, and Lay). 2019.

[40] SFS-EN ISO 4287. Geometrical product specifications (GPS). Surface texture: Profile method. Terms, definitions and surface texture parameters. 1999.

[41] Wittcoff, H. A. et. al. Industrial Organic Chemicals (3rd Edition). John Wiley & Sons. p. 284. 2013.

[42] Biron, M. Material Selection for Thermoplastic Parts - Practical and Advanced Information for Plastics Engineers. Elsevier. 2016.

[43] Osswald, T. et. al. International Plastics Handbook - The Resource for Plastics Engineers (4th Edition). Hanser Publishers. Table A.12. p. 735. 2006.

[44] Subramanian, M. N. Polymer Blends and Composites - Chemistry and Technology. John Wiley & Sons. p. 27. 2017.

[45] Resistivity, conductivity and temperature coefficient of various materials at 20 °C. https://en.wikipedia.org/wiki/Electrical_resistivity_and_conductivity. Retrieved 19.8.2020.

[46] Prusa, J. Prusa Research: The Original Prusa i3 MK3S 3D Printer. https://www.prusa3d.com/original-prusa-i3-mk3/. Retrieved 4.2.2020.

[47] Michler, G. H. Atlas of Polymer Structures - Morphology, Deformation and Fracture Structures. Hanser Publishers. p. 27-28. 2016.

[48] Buj-Corral, I. et. al. Influence of infill and nozzle diameter on porosity of FDM printed parts with rectilinear grid pattern. Proceria Manufacturing. Elsevier. No. 41. p. 288-295. 2019.

[49] Pérez, M. et. al. Surface Quality Enhancement of Fused Deposition Modeling (FDM) Printed Samples Based on the Selection of Critical Printing Parameters. Materials 11. 1382. Special Issue of the Manufacturing Engineering Society (MES). 2018.

[50] Anitha, R. et. al. Critical parameters influencing the quality of prototypes in fused deposition modelling. Journal of Materials Processing Technology. Vol. 118, (1–3). p. 385–388. 2001.

[51] Horvath, D. et. al. Improvement of surface roughness on ABS 400 polymer using design of experiments (DOE). Materials Science Forum 561. p. 2389–2392. 2007.

[52] Nancharaiah, T. et. al. An experimental investigation on surface quality and dimensional accuracy of FDM components. International Journal on Emerging Technologies. Vol. 1(2). p. 106–111. 2010.

[53] Chaidas, D. et. al. The impact of temperature changing on surface roughness of FFF process. IOP Conference Series: Materials Science and Engineering. Vol. 161 (1). Art. no. 012033. 2016.

[54] You, D.-H. Optimal printing conditions of PLA printing material for 3D printer. Transactions of the Korean Institute of Electrical Engineers. Vol. 65 (5), p. 825-830. 2016.

[55] Valerga, A. P. et. al. Preliminary study of the influence of manufacturing parameters in fused deposition modelling. Proceedings of the 26th DAAAM International Symposium, p.1004-1008. 2015.

[56] Dev, S. et. al. Experimental investigation and optimization of FDM process parameters for material and mechanical strength. Materials Today: Proceedings. Vol. 26. Part 2. p. 1995-1999. 2020.

[57] Hodgson, G. Flow Math. Slic3r Manual. https://manual.slic3r.org/advanced/flow-math. Retrieved 6.8.2020.

APPENDIX A

The data sheet of PrePerm® ABS450 filament

TECHNICAL DATASHEET TP20280 – APR. 2019

PREMIX

PREPERM® ABS450

ε_r = 4.5, tan δ = 0.0042 Applications: 3D-filaments

PREPERM® ABS450 is a special compound based on Premix proprietary ABS technology. It offers a stable dielectric constant over wide frequency and temperature ranges with low losses. ABS450 is optimized for extrusion but it can also be injection molded.

Dielectric properties

		Standard	Value	Tolerance
Dielectric constant, ε_r	2.4 GHz	SPDR	4.5	±0.15
Loss tangent, tan δ	2.4 GHz	SPDR	0.0042	-

Processing parameters

		Unit	Value
Injection moulding			
	Material temperature	°C	210 – 240
	Mould temperature	°C	60 – 90
	Injection pressure		Moderate
	Injection speed		Moderate
Extrusion			
	Material temperature	°C	200 – 240
	Die temperature	°C	200 – 250
	Tool/roll temperature	°C	50 – 90

These temperatures can be used for guidance purposes. Processing temperature is also dependent on the equipment used. The instructions of the equipment manufacturer should be followed.

Pre-drying in a dehumidifying drier is recommended e.g. 2 - 4 hours at 80 - 90°C. If a dehumidified drier is not available, we recommend increasing the drying temperature to 90 - 100 ° C and prolonging the drying time to 3 to 6 hours. If moisture level is too high, it can be seen in surface quality, but it does not cause polymer degradation.

www.preperm.com

APPENDIX B

Indexing, edge thickness and mesh size of the cubes of the 1st set

Cube	Edge thick-ness [mm]	Triangle max. length [mm]	Triangle min. length [mm]	Triangle median length [mm]
1.1a	2.51	8.36	3.12	5.35
1.1b	1.95	6.50	3.71	4.96
1.2a	2.12	8.36	3.12	5.35
1.2b	1.65	6.50	3.71	4.96
2.1a	3.12	10.39	5.01	7.10
2.1b	2.69	8.98	4.63	6.58
2.2a	2.64	10.39	5.01	7.10
2.2b	2.28	8.98	4.63	6.58
2.3a	2.23	10.39	5.01	7.10
2.3b	1.92	8.98	4.63	6.58
3.1a	1.84	6.12	2.60	4.15
3.2b	1.40	4.68	2.64	3.56
solid				

APPENDIX C

The effect of the electrolyte gel to the resistance of the object

The resistance of the cube 2.1a measured in top-bottom direction using thick electrodes

	No gel [kΩ]	Gel [kΩ]
1	142.3	65.5
2	127.0	63.7
3	126.5	72.4
4	126.0	57.4
5	126.3	76.8
6	124.8	51.5
7	128.4	63.0
8	127.6	54.2
9	127.8	69.8
10	121.2	54.1
11	120.7	71.1
12	125.0	52.7
13	128.0	66.7
14	129.1	55.7
15	129.1	77.5
16	124.9	51.6
17	118.8	44.5
18	124.1	58.2
19	124.3	43.7
20	123.2	57.3
21	123.0	46.3
Avg.	126.1	59.7
St. Dev.	4.6	10.1
COV	3.7	17.0

APPENDIX D

Measured dimensions of the objects of 1st and 2nd set

	Cube	Dimension A [mm]	Dimension B [mm]	Dimension C [mm]	Weight [g]
1st set	1.1a	26.28	26.25	26.32	12.4
	1.1b	25.81	25.57	25.62	9.1
	1.2a	25.90	26.02	25.98	9.4
	1.2b	25.80	25.33	25.44	6.8
	2.1a	26.85	26.60	26.55	10.9
	2.1b	26.40	26.08	26.05	10.3
	2.2a	26.42	26.18	26.35	8.3
	2.2b	26.01	26.32	25.91	7.9
	2.3a	25.94	26.09	26.03	6.0
	2.3b	25.60	25.60	25.60	5.6
	3.1a	25.93	25.83	25.79	10.5
	3.2b	25.25	25.18	25.17	8.8
	solid	29.00	29.79	29.75	14.8
2nd set	1_1_10	27.27	27.29	26.86	12.12
	1_1_15	27.26	27.34	27.15	11.90
	1_1_15_T	27.34	27.31	27.21	12.45
	1_1_30	27.22	27.26	27.00	11.68
	solid_10	24.86	24.84	24.92	15.18
	solid_15	24.42	24.71	24.73	15.24
	solid_15_T	24.47	24.64	24.72	14.64
	solid_30	24.49	24.62	24.91	15.44

APPENDIX E

Surface roughness measurement results and pictures of the surface quality. The results are expressed in micrometres [µm].

Cube	10	15	15_T	30
1	26.05	35.81	43.67	70.88
2	28.22	37.98	40.53	70.84
3	27.12	36.94	40.39	74.20
4	29.30	36.94	40.39	73.02
5	29.28	38.02	39.30	78.91
6	28.20	37.98	40.41	82.90
7	28.22	38.02	41.49	77.62
8	28.20	37.98	40.41	81.73
9	28.22	41.23	39.30	86.17
10	29.30	36.89	43.72	83.99
11	28.20	37.98	39.32	79.59
12	31.47	40.15	40.41	80.68
AVG.	28.5	38.0	40.8	78.4
St. Dev.	1.32	1.46	1.50	5.14
COV	4.63	3.83	3.68	6.56

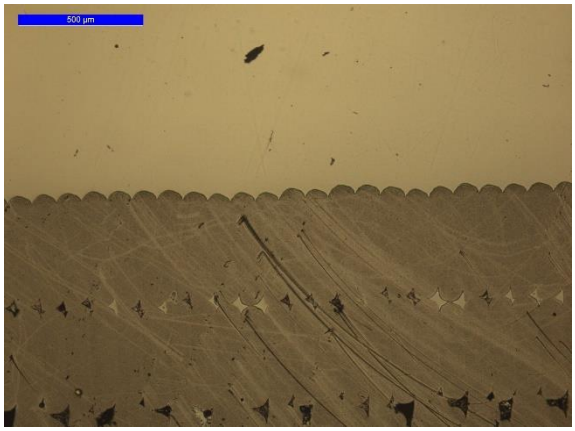

Cube 10

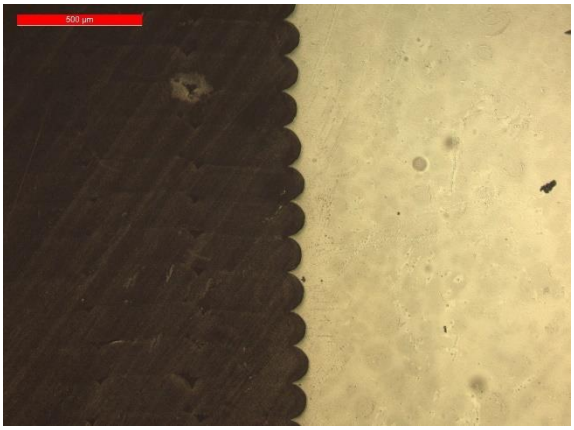

Cube 15

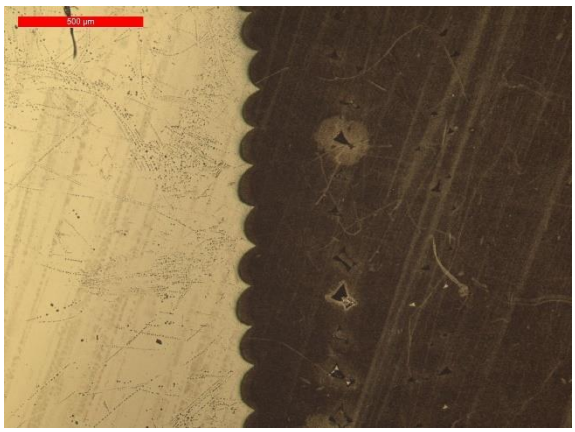

Cube 15_T

Cube 30

APPENDIX F

8-bit pictures for the empty space and degree of filling determination of the solid cubes of the 2nd set. The yellow line indicates the line of the filling degree measurement. The pictures were taken using the same magnification, although the scale bar is missing from the picture Cube 15_T horizontal.

Cube 10 horizontal

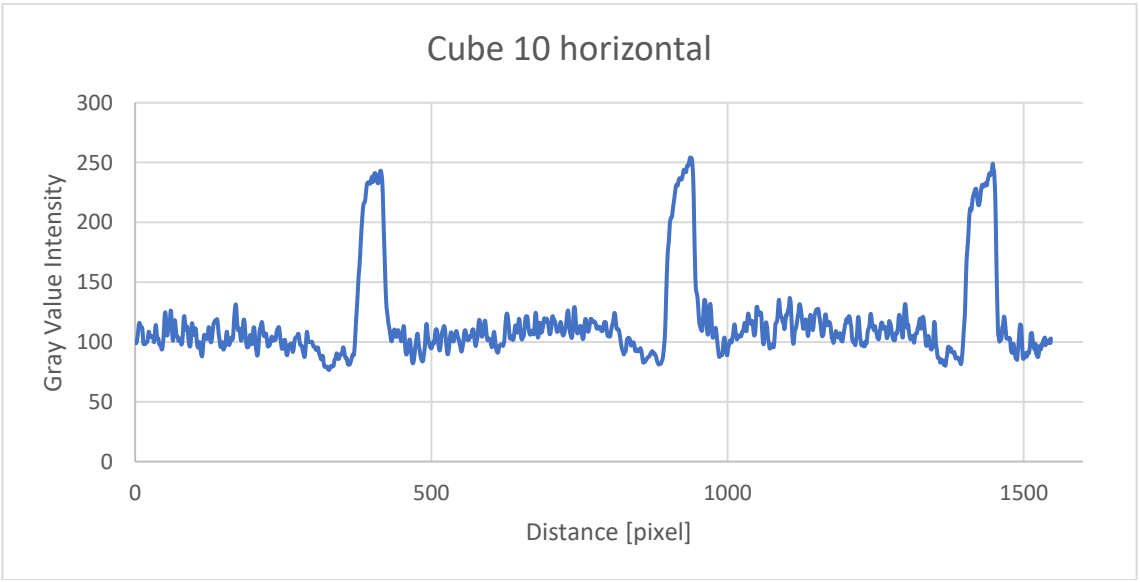

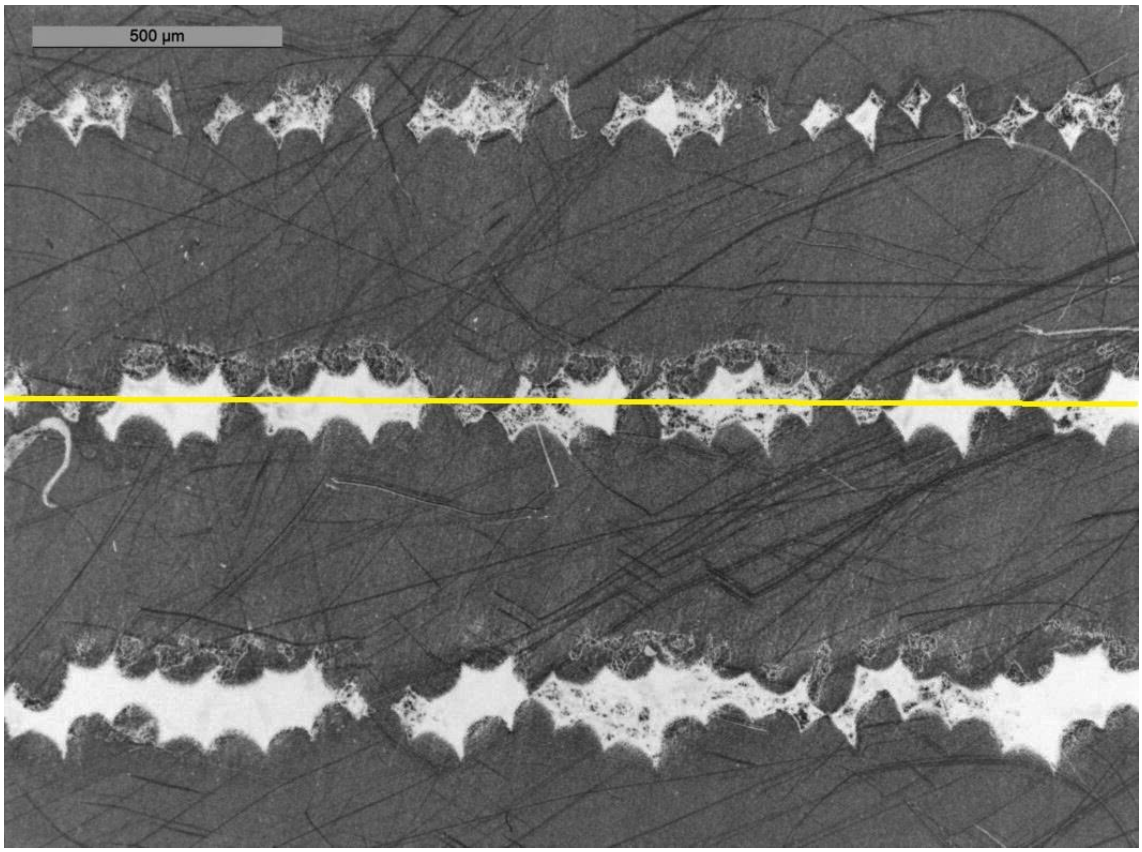

Cube 10 vertical

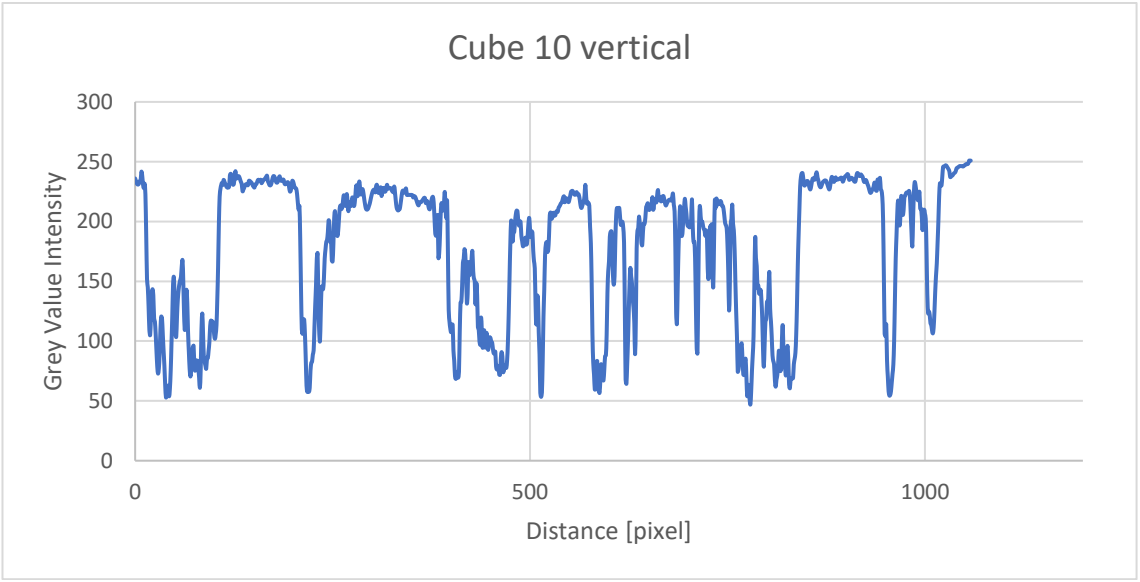

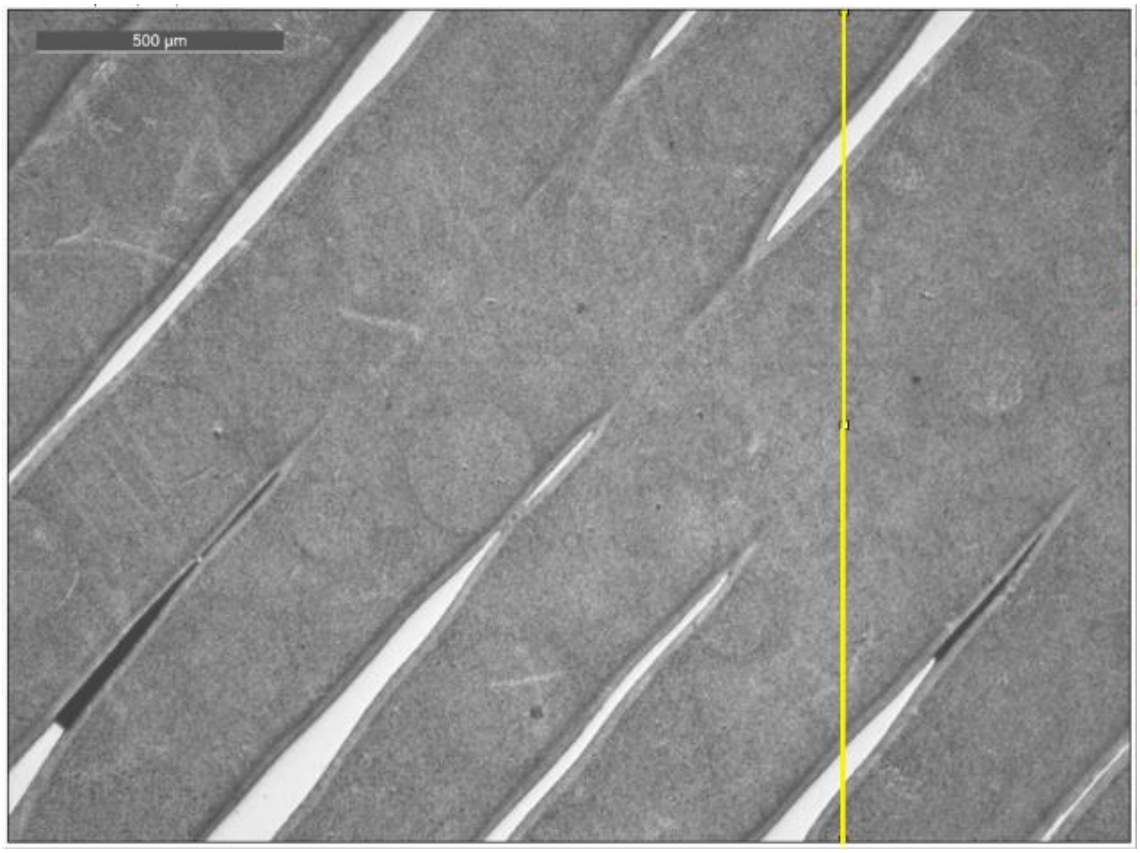

Cube 15 horizontal

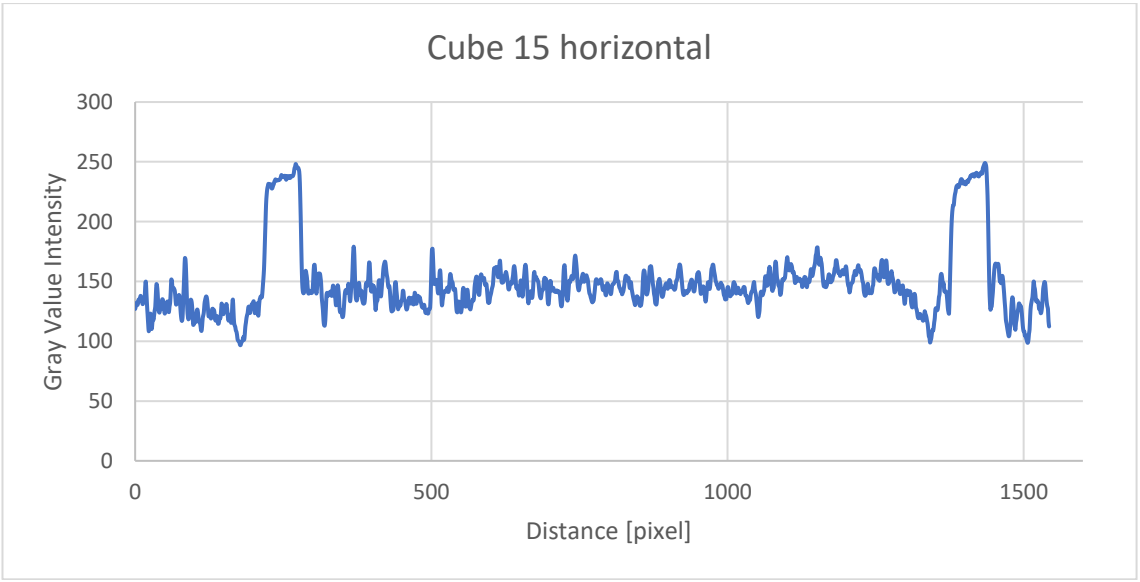

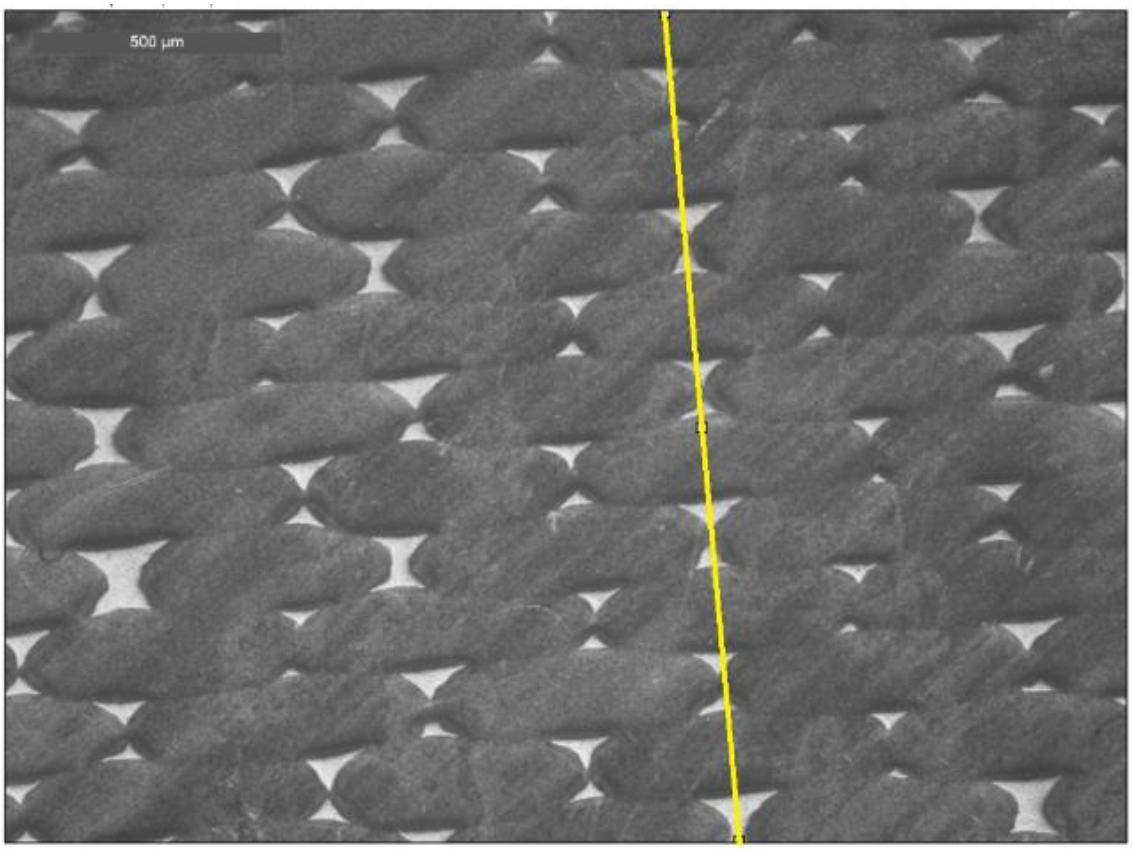

Cube 15 vertical

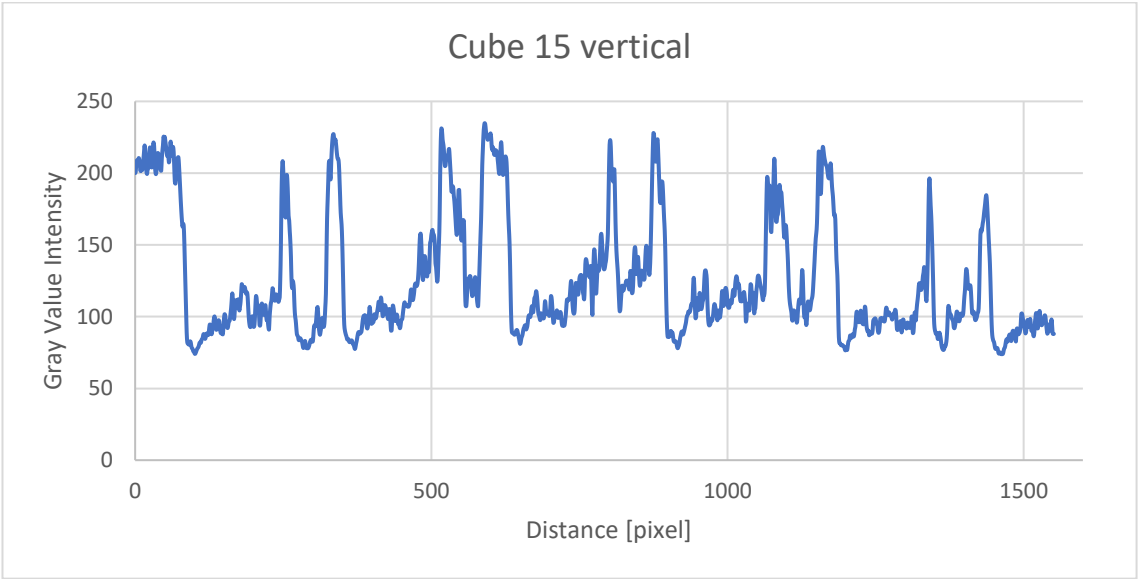

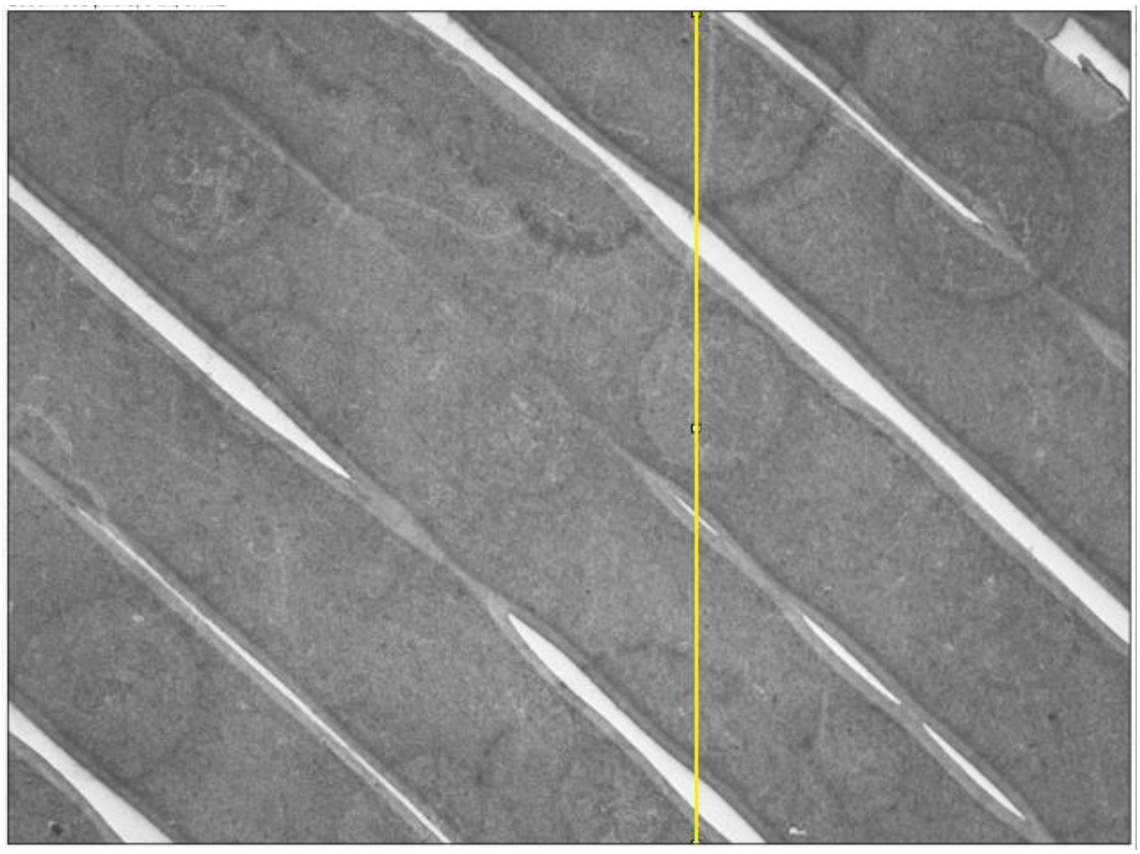

Cube 15_T horizontal

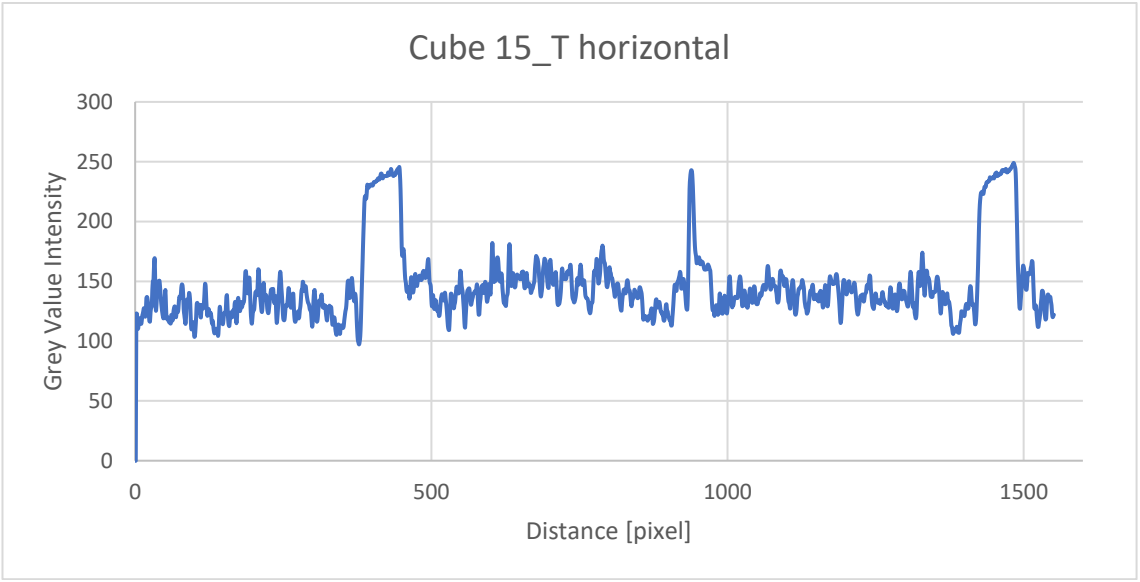

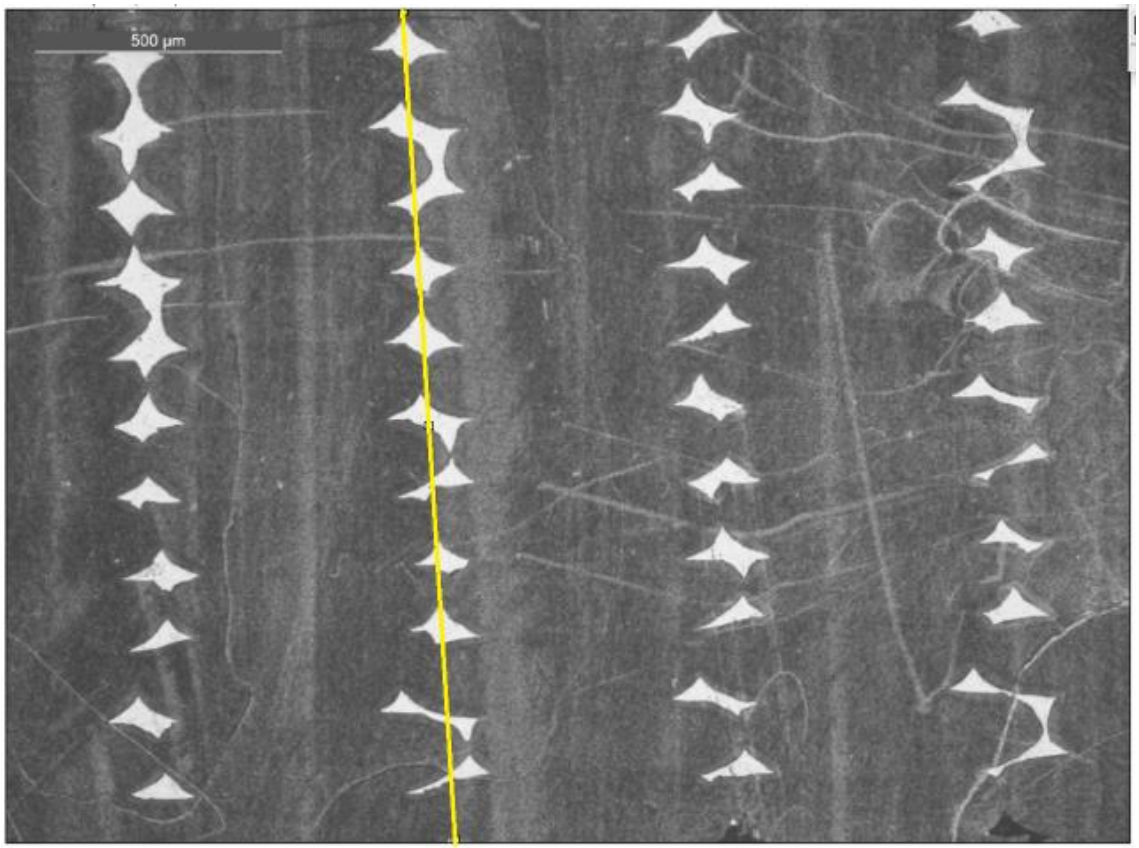

Cube 15_T vertical

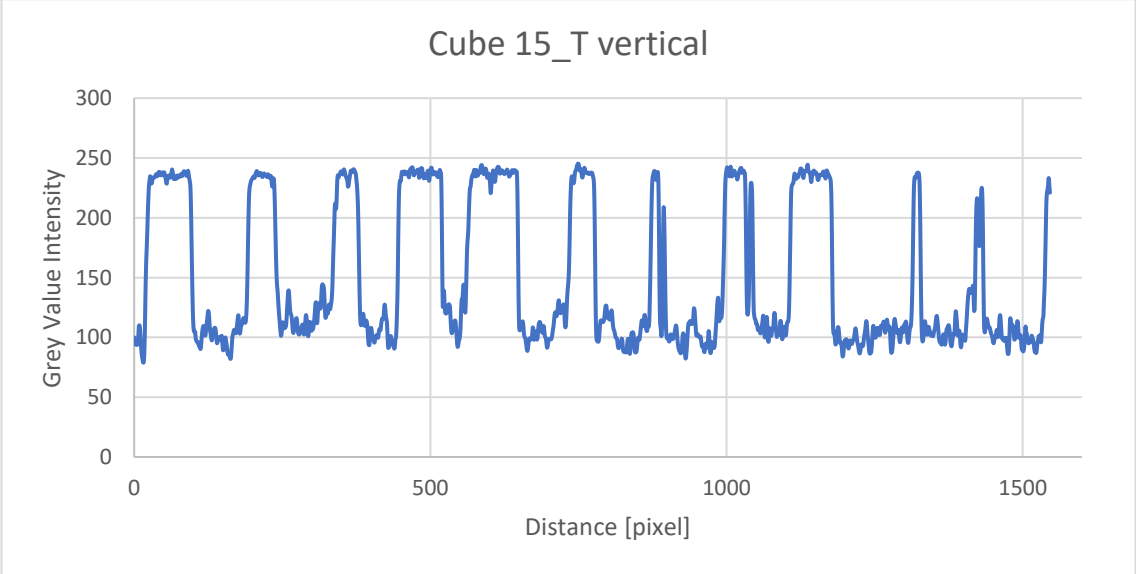

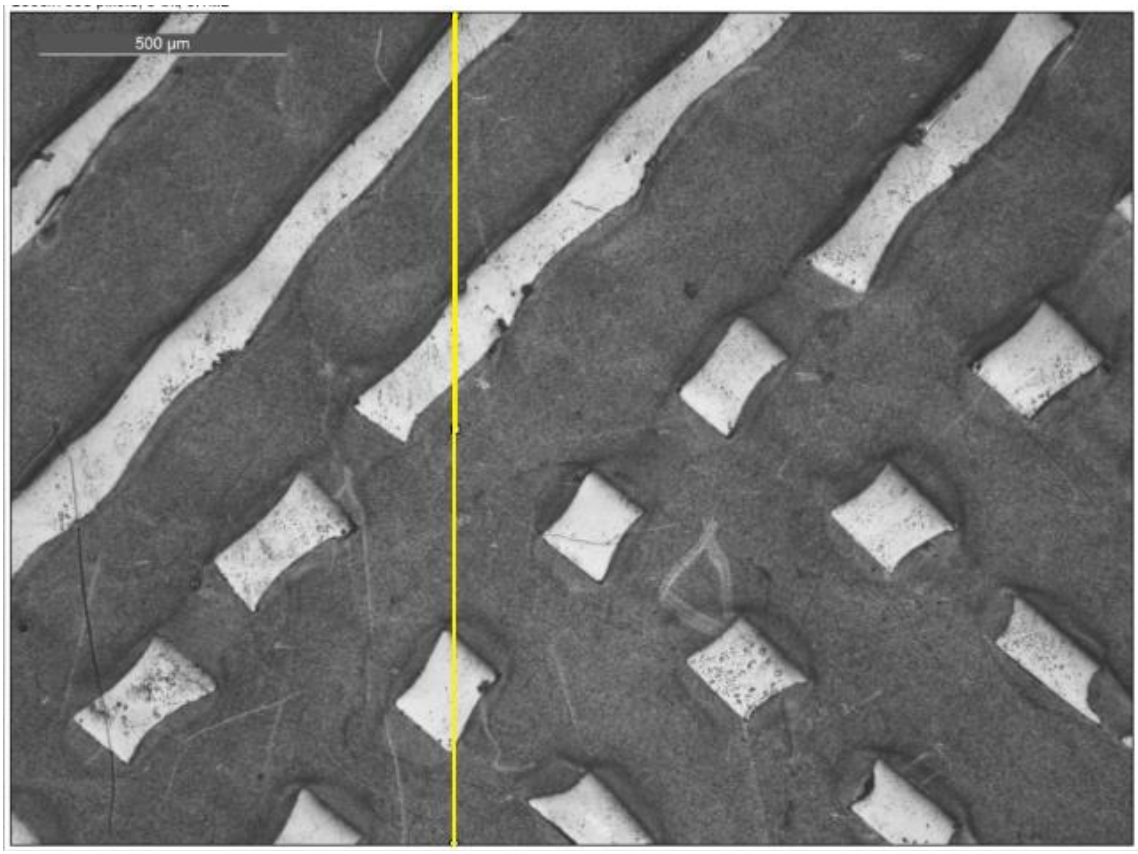

Cube 30 horizontal

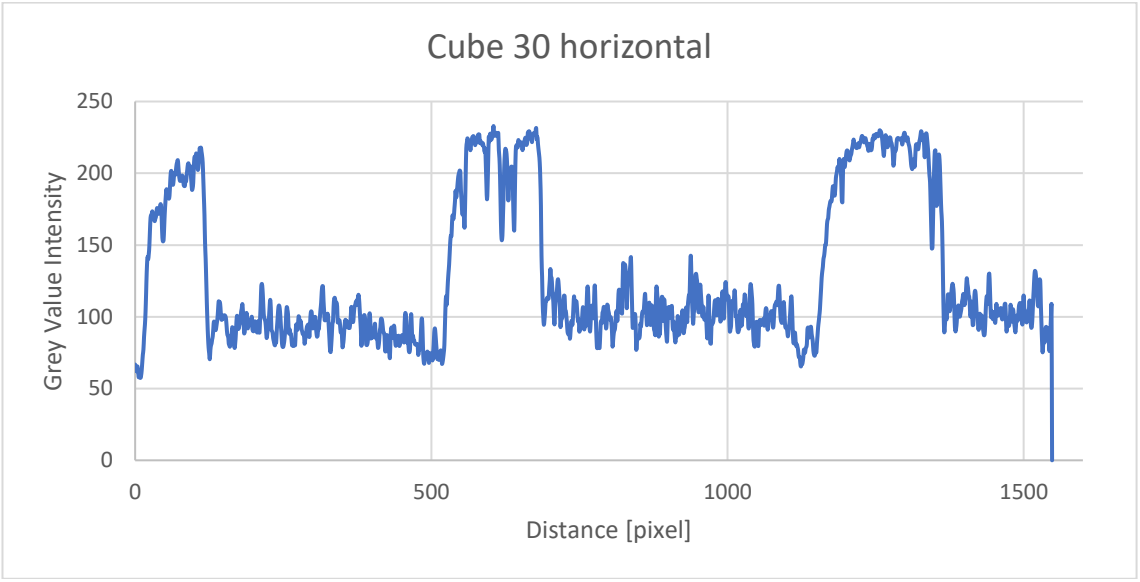

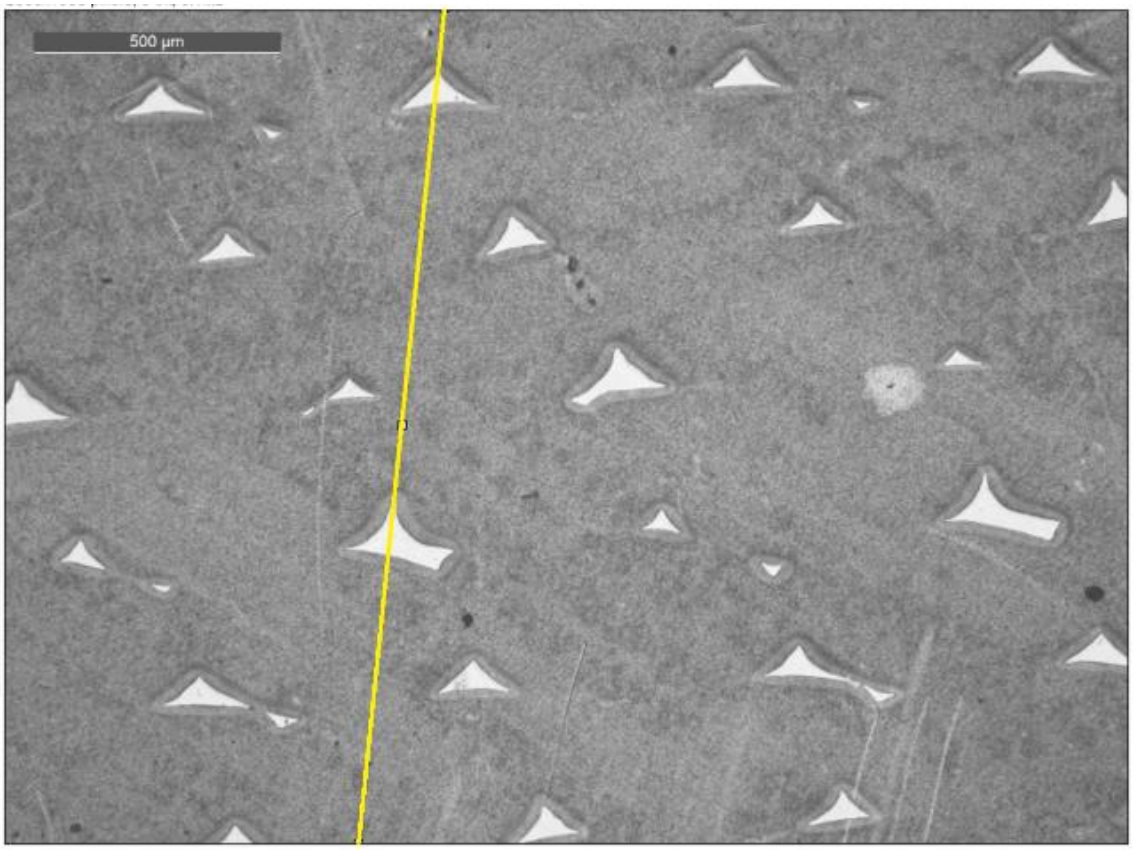

Cube 30 vertical

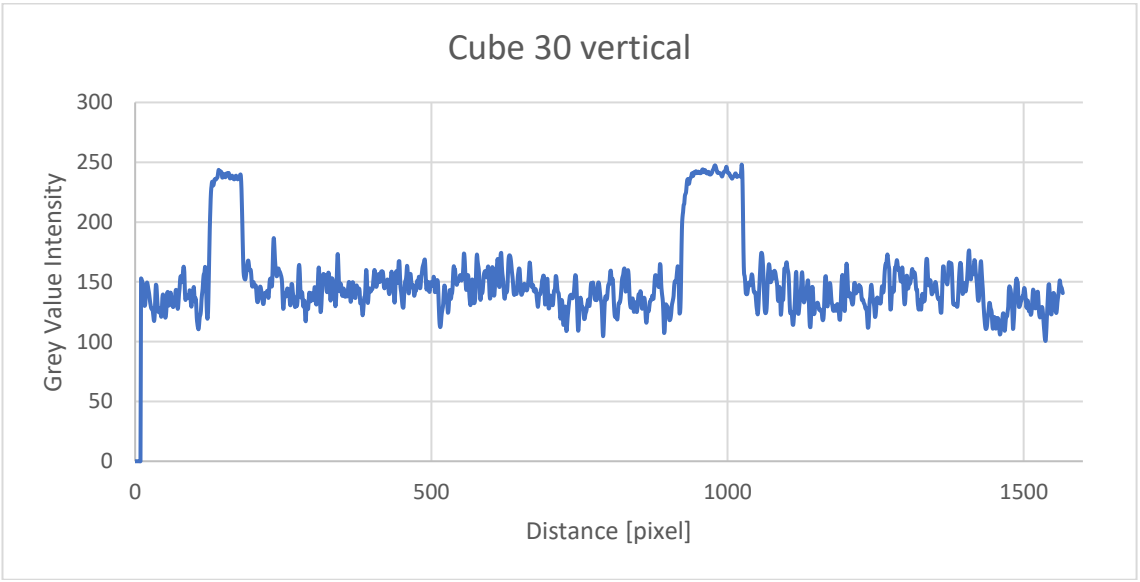

APPENDIX G

Pictures of the cross-cuts of the solid spheres

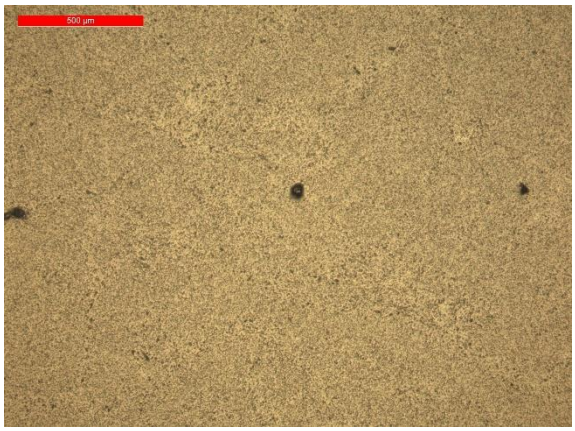

Sphere 10, both horizontal and vertical cross-cut looked similar

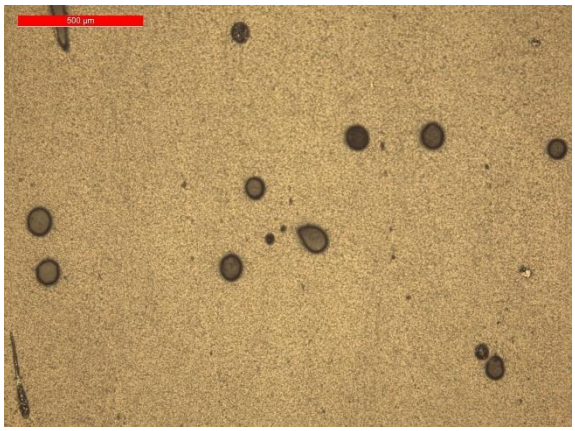

Sphere 15 horizontal

Sphere 15 vertical

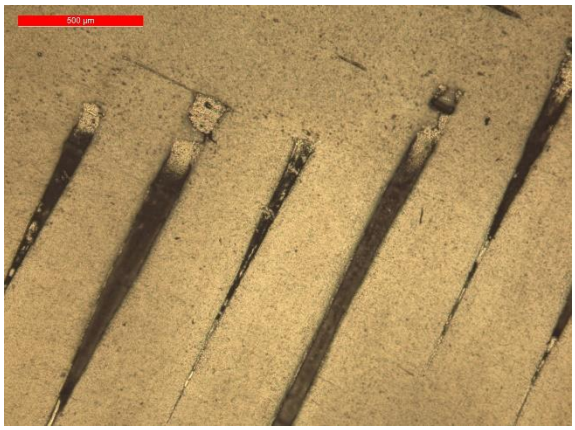

Sphere 15_T horizontal

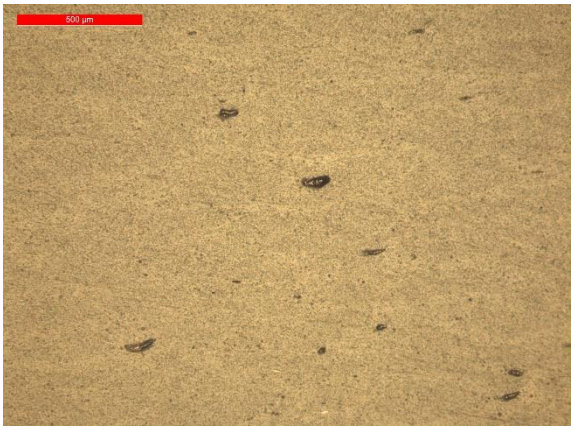

Sphere 15_T vertical

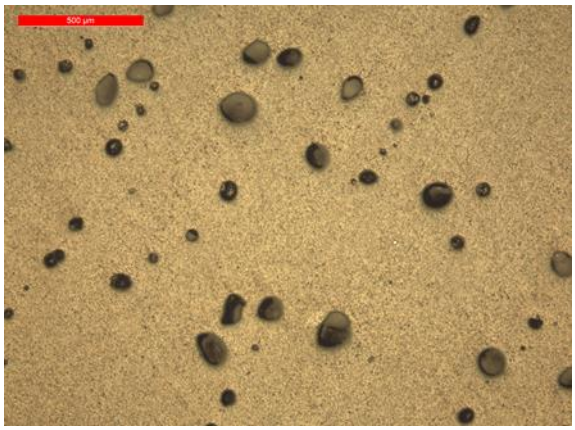

Sphere 30 horizontal

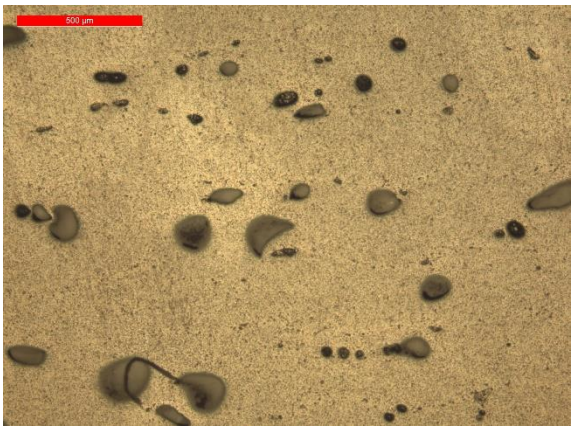

Sphere 30 vertical

APPENDIX H

Average amount of empty space between layers and average degree of filling of the solid cubes of the 2nd set

Cube	Orienta-tion	Empty space in orientation [%]	Avg. empty space [%]	Degree of filling in orientation [%]	Avg. degree of filling [%]
10	Horizontal Vertical	8.6 9.7	9.2	91.3 52.6	72.0
15	Horizontal Vertical	4.1 3.5	3.8	91.5 82.3	86.9
15_T	Horizontal Vertical	4.9 4.9	4.9	90.4 65.6	78.0
30	Horizontal Vertical	15.1 2.0	8.6	74.7 89.4	82.0

Average amount of empty space between layers in the solid spheres

Sphere	Orientation	Empty space [%]	Avg. empty space [%]
10	Horizontal Vertical	< 1 < 1	< 1
15	Horizontal Vertical	3.3 1.0	2.2
15_T	Horizontal Vertical	8.5 1.2	4.9
30	Horizontal Vertical	6.6 6.8	6.7

APPENDIX I

Resistance measurement results of the 1st set

Cube	Orientation	Resistance [kΩ]	Resistivity [Ω·cm]
1.1A	Top-bottom	1.18	2950
	Side-side	3.263	8158
1.1B	Top-bottom	1.01	2525
	Side-side	3.04	7600
1.2A	Top-bottom	2.552	6380
	Side-side	2.33	5825
1.2B	Top-bottom	3.94	9850
	Side-side	-	-
2.1A	Top-bottom	3.98	9950
	Side-side	2.37	5925
2.1B	Top-bottom	3.353	8383
	Side-side	10.9	27250
2.2A	Top-bottom	4.408	11020
	Side-side	3.827	9568
2.2B	Top-bottom	2.19	5475
	Side-side	2.158	5395
2.3A	Top-bottom	2.152	5380
	Side-side	5.232	13080
2.3B	Top-bottom	6.97	17425
	Side-side	4.77	11925
3.1A	Top-bottom	1.935	4838
	Side-side	6.05	15125
3.2B	Top-bottom	2.967	7418
	Side-side	4.195	10488
solid	Top-bottom	0.0734	184
	Side-side	0.0619	155

APPENDIX J

Resistance measurement results of the 2nd set

	Cube	Orientation	Resistance [Ω]	Resistivity [Ω·cm]
Solid	10	Top-bottom	387	968
		Side-side	125	313
	15	Top-bottom	118	295
		Side-side	70	175
	15_T	Top-bottom	227	567
		Side-side	105	262
	30	Top-bottom	128	320
		Side-side	33	82
Mesh	10	Top-bottom	679	1698
		Side-side	2462	6155
	15	Top-bottom	894	2235
		Side-side	1438	3595
	15_T	Top-bottom	1454	3635
		Side-side	1778	4445
	30	Top-bottom	643	1608
		Side-side	713	1783

APPENDIX K

Resistance measurement results of the cubes with different infill patterns

	Infill [%]	Orientation	Resistance [Ω]	Resistivity [Ω·cm]
Honeycomb	90	Top-bottom	733	1833
		Side-side	141	353
	80	Top-bottom	1841	4603
		Side-side	150	375
	70	Top-bottom	2412	6030
		Side-side	154	385
	60	Top-bottom	1973	4933
		Side-side	156	390
	50	Top-bottom	1308	3270
		Side-side	159	398
	40	Top-bottom	2496	6240
		Side-side	173	433
Rectilinear	100	Top-bottom	1150	2875
		Side-side	125	313
	90	Top-bottom	2080	5200
		Side-side	168	420
	80	Top-bottom	1506	3765
		Side-side	148	370
	70	Top-bottom	1823	4558
		Side-side	179	448
	60	Top-bottom	1701	4253
		Side-side	165	413
	50	Top-bottom	2100	5250
		Side-side	208	520
3D Honeycomb	50	Top-bottom	779	1948
		Side-side	168	420
	40	Top-bottom	2342	5855
		Side-side	194	485
	30	Top-bottom	2054	5135
		Side-side	175	438
	20	Top-bottom	728	1820
		Side-side	208	520
	10	Top-bottom	1842	4605
		Side-side	278	695

APPENDIX L

Cube	Orientation	Empty space in orientation [%]	Avg. empty space [%]	Degree of filling in orientation [%]	Avg. degree of filling [%]	Resistivity in orientation [Ω·cm]	Avg. resistivity [Ω·cm]
10	Horizontal	8.6	9.2	91.3	72.0	968	641
	Vertical	9.7		52.6		313	
15	Horizontal	4.1	3.8	91.5	86.9	295	235
	Vertical	3.5		82.3		175	
15_T	Horizontal	4.9	4.9	90.4	78.0	567	414
	Vertical	4.9		65.6		262	
30	Horizontal	15.1	8.6	74.7	82.0	320	201
	Vertical	2.0		89.4		82	

APPENDIX M

Calculated permittivity results of the solid spheres

Sphere	Degree of filling	Real part	Imaginary part	Permittivity
10	1	4.500	0.019	4.519
15	0.978	4.389	0.018	4.407
15_T	0.951	4.255	0.017	4.272
30	0.933	4.167	0.017	4.184